nature communications

Article

https://doi.org/10.1038/s41467-024-51881-x

PTPN14 aggravates neointimal hyperplasia via boosting PDGFRβ signaling in smooth muscle cells

Received: 10 November 2023

Accepted: 20 August 2024

Published online: 27 August 2024

Check for updates

Qiannan Ma[1,2,5], Xue He[1,5], Xue Wang[1], Guobing Zhao[1], Yanhong Zhang[1], Chao Su[3], Minxin Wei[3], Kai Zhang[4], Ming Liu[2] ✉, Yi Zhu[1,2] ✉ & Jinlong He[1] ✉

Smooth muscle cell (SMC) phenotypic modulation, primarily driven by PDGFRβ signaling, is implicated in occlusive cardiovascular diseases. However, the promotive and restrictive regulation mechanism of PDGFRβ and the role of protein tyrosine phosphatase non-receptor type 14 (PTPN14) in neointimal hyperplasia remain unclear. Our study observes a marked upregulation of PTPN14 in SMCs during neointimal hyperplasia. PTPN14 overexpression exacerbates neointimal hyperplasia in a phosphatase activity-dependent manner, while SMC-specific deficiency of PTPN14 mitigates this process in mice. RNA-seq indicates that PTPN14 deficiency inhibits PDGFRβ signaling-induced SMC phenotypic modulation. Moreover, PTPN14 interacts with intracellular region of PDGFRβ and mediates its dephosphorylation on Y692 site. Phosphorylation of PDGFRβ^{Y692} negatively regulates PDGFRβ signaling activation. The levels of both PTPN14 and phospho-PDGFRβ^{Y692} are correlated with the degree of stenosis in human coronary arteries. Our findings suggest that PTPN14 serves as a critical modulator of SMCs, promoting neointimal hyperplasia. PDGFRβ^{Y692}, dephosphorylated by PTPN14, acts as a self-inhibitory site for controlling PDGFRβ activation.

Vascular smooth muscle cells (VSMCs) are the predominant constituents of arteries and play a fundamental role in maintaining the normal physiological functions of blood vessels. In response to pathological stimuli or vascular injury, VSMCs migrate to the subintima and undergo pathological proliferation, inducing stenosis in the vascular lumen and then causing vascular restenosis, thereby contributing to the development of atherosclerosis and restenosis[1,2]. Growth factors, such as platelet-derived growth factor (PDGF), basic fibroblast growth factor (bFGF), and transforming growth factor-β (TGF-β), are key mediators to induce VSMC phenotype modulation[3,4]. During neointima formation, PDGF is locally produced and initiates a multitude of biological effects through the activation of its receptor PDGFRβ and subsequent intracellular signaling that contribute to VSMC proliferation, migration, and dedifferentiation[5]. Although numerous studies have demonstrated the central role of PDGFRβ and elucidated the downstream signaling of PDGFRβ, the precise regulatory mechanisms governing PDGFRβ signaling, both in terms of its promotion and inhibition, remain largely unknown.

Protein tyrosine phosphorylation, which is balanced by tyrosine kinases and protein tyrosine phosphatases (PTPs), is intimately

[1]Tianjin Key Laboratory of Metabolic Diseases, Province and Ministry Co-sponsored Collaborative Innovation Center for Medical Epigenetics, Department of Physiology and Pathophysiology, Tianjin Medical University, Tianjin 300070, China. [2]Department of Endocrinology and Metabolism, Tianjin Research Institute of Endocrinology, Tianjin Medical University General Hospital, Tianjin 300052, China. [3]Division of Cardiovascular Surgery, Cardiac and Vascular Center, The University of Hong Kong-Shenzhen Hospital, Shenzhen 518040, China. [4]Department of Biochemistry and Molecular Biology, School of Basic Medical Sciences, Tianjin Medical University, Tianjin 300070, China. [5]These authors contributed equally: Qiannan Ma, Xue He. ✉e-mail: mingliu@tmu.edu.cn; zhuyi@tmu.edu.cn; hejinlong@tmu.edu.cn

associated with various processes, including proliferation, migration, and differentiation. PTP non-receptor type 14 (PTPN14), also known as Pez, PTP36, or PTPD2, belongs to the classical phosphotyrosine-specific phosphatase family[6]. PTPN14 was first detected in normal human breast tissue in 1995 and is widely expressed in various tissues, including the skeletal muscle, kidney, lung, and placenta[7]. It is characterized by an N-terminal FERM domain (band 4.1, ezrin, radixin, and moesin) that is related to the cell cytoskeleton, a middle linker region that contains a PPxY domain that interacts with other proteins containing the WW domain, and a C-terminal-conserved PTP domain that is involved in catalytic phosphorylation[8]. Previous studies have reported that PTPN14 is involved in the occurrence and development of various cancers by regulating cell migration, metastasis, adhesion, and turnover[9–11]. Moreover, we have recently reported that PTPN14 inhibited the disturbed flow-induced athero-prone phenotype of endothelial cells (ECs)[12]. Despite these findings, the role of PTPN14 in VSMCs and neointimal hyperplasia remains unclear.

Herein, we observed unexpectedly high PTPN14 expression during VSMC phenotypic modulation and demonstrated the critical role of PTPN14 in promoting VSMC dedifferentiation with gain- and loss-of-function in vitro and in vivo experiments. We also revealed that PTPN14 could dephosphorylate PDGFRβ at Y692 site, a previously unidentified self-inhibitory site of PDGFRβ, resulting in boosting PDGF-BB/PDGFRβ signaling in VSMCs and exacerbating neointimal hyperplasia.

Results

PTPN14 expression was induced in VSMCs during neointimal hyperplasia

We have previously reported that PTPN14 negatively regulates disturbed flow-induced endothelial activation[12]. We constructed a mouse model of disturbed flow-related atherosclerosis by partially ligating the carotid arteries. Unexpectedly, we found that PTPN14 expression was markedly induced in the neointima of the hyperplastic part of the vessel compared to that in the non-hyperplastic part (Fig. 1A). To determine whether PTPN14 expression is elevated during VSMC phenotypic modulation, human aortic SMCs (HA-VSMCs) were stimulated with PDGF-BB at different times and doses. Results revealed that PTPN14 expression were both time- and dose-dependently elevated by PDGF-BB in parallel with the expression of the proliferative VSMC marker PCNA, whereas the expression of contractile VSMC markers, including CNN1, α-SMA, and SM22, was significantly reduced (Supplementary Fig. 1A–D). Additionally, we found that PDGF-BB treatment did not affect the mRNA level of PTPN14 in VSMCs (Supplementary Fig. 1E), indicating that PDGF-BB may induce the expression of PTPN14 through a post-transcriptional mechanism. Consistently, we observed that the presence of PDGF-BB enhanced the stability of PTPN14 protein in VSMCs (Supplementary Fig. 1F, G).

To further confirm the regulation of PTPN14 in vivo, we constructed two mouse models of neointimal hyperplasia and determined the expression of PTPN14 in VSMCs. Consistently, in both wire-mediated carotid artery injury and carotid artery ligation models, PTPN14 expression was strongly induced in the neointima on days 14 and 21 after surgery (Fig. 1B, C and Supplementary Fig. 2A, B). Moreover, western blot analysis with left carotid arteries (LCAs) demonstrated an elevation in PTPN14 expression on both days 14 and 21 after wire injury in parallel with upregulation of OPN and downregulation of contractile VSMC markers including CNN1, α-SMA, and SM22 (Fig. 1D, E). Additionally, the mRNA levels of PTPN14 were not affected in injured arteries (Supplementary Fig. 2C).

Next, we examined the expression of PTPN14 in human coronary arteries. Coronary artery sections were divided into three groups according to the degree of stenosis: non-hyperplastic, moderately hyperplastic, and severely hyperplastic vessels (Fig. 1F). We found that PTPN14 was abundant in the neointima of vessels and was positively correlated with the development of hyperplasia. PTPN14 expression in the neointima was higher in the moderate and severe hyperplasia groups than that in the non-hyperplasia group (Fig. 1G, H). Together, these in vitro and in vivo data demonstrate that PTPN14 expression is induced in proliferative VSMCs and provide a critical clue to the link between PTPN14 and neointimal hyperplasia.

PTPN14 aggravated neointimal hyperplasia in a phosphatase activity-dependent manner

Next, we examined whether PTPN14 promoted neointima formation in mice. Mice were subjected to wire injury in the LCAs and simultaneously infected with PTPN14 (AdPTPN14) or scrambled (AdNC) adenovirus, as previously described[13]. Immunofluorescence staining of the LCAs and right carotid arteries (RCAs) confirmed their overexpression in VSMCs (Supplementary Fig. 3A–C). Compared to RCAs, forced expression of PTPN14 promoted neointima formation with increased ratio of intima to lumen in LCAs 14 d after injury, whereas it had minimal effects on the circumference of the external elastic lamina (Fig. 2A, B). Although PTPN14 overexpression did not alter the number of proliferating PCNA-positive cells in the RCAs, it increased the number in the wire-injured LCAs (Fig. 2C, D). Moreover, western blot analysis with the lysate of LCAs further confirmed that PTPN14 overexpression upregulated the expression of PCNA, OPN, VIM and downregulated that of contractile VSMC markers, including α-SMA and SM22 (Fig. 2E, F).

As a member of the classical tyrosine phosphatase family, PTPN14 carries out its catalytic function by dephosphorylating its substrate[14,15]. To investigate whether the impact of PTPN14 on neointimal hyperplasia relies on its phosphatase activity, we mutated the cysteine of PTPN14 at site 1121 to serine ($PTPN14^{C1121S}$) to inactivate its phosphatase activity, as previously reported[8,16]. In contrast to the effects of wild-type PTPN14, $PTPN14^{C1121S}$ overexpression attenuated neointima formation in the LCAs 14 d after injury, resulting in a lower ratio of intima to lumen compared with that in the control group (Fig. 2A, B). $PTPN14^{C1121S}$ overexpression barely affected the morphology of RCAs or circumference of the external elastic lamina in LCAs (Fig. 2A, B). Besides, $PTPN14^{C1121S}$ overexpression decreased the number of proliferating PCNA-positive cells in LCAs, while had no obvious effect on RCAs (Fig. 2C, D). Moreover, $PTPN14^{C1121S}$ overexpression reduced the PCNA, OPN, VIM and increased the expression of α-SMA and SM22 in injured LCAs compared to those in the control group (Fig. 2E, F). In addition, we observed that $PTPN14^{C1121S}$ overexpression led to a notable reduction in the phosphatase activity of PTPN14 in the injured LCAs when compared to the AdNC groups (Supplementary Fig. 3D). Thus, our results suggest that PTPN14 exacerbates neointimal hyperplasia in a phosphatase activity-dependent manner.

PTPN14 promoted PDGF-BB-induced VSMC migration, proliferation, and dedifferentiation

SMCs display considerable plasticity that upon stimulation by dedifferentiation factors, such as PDGF-BB, and they undergo phenotype transformation from a stable fully differentiated contractile phenotype to a dedifferentiated synthetic phenotype, which is manifested as a loss of differentiation markers, accompanied by increased migration and proliferation ability[17]. We further examined the potential role of PTPN14 in PDGF-BB-induced cell migration, proliferation, and dedifferentiation. PTPN14 or $PTPN14^{C1121S}$ was forcibly overexpressed in VSMCs using adenoviruses (Supplementary Fig. 4A, B). Consistent with our in vivo results, we observed that $PTPN14^{C1121S}$ overexpression significantly diminished the phosphatase activity of PTPN14 in VSMCs compared to that in the AdNC groups (Supplementary Fig. 4C). To evaluate the effect of PTPN14 on VSMC migration, we performed scratch and Transwell assays. Under baseline conditions, PTPN14 overexpression promoted VSMC migration, whereas $PTPN14^{C1121S}$ overexpression did not have any significant effect (Fig. 3A, D).

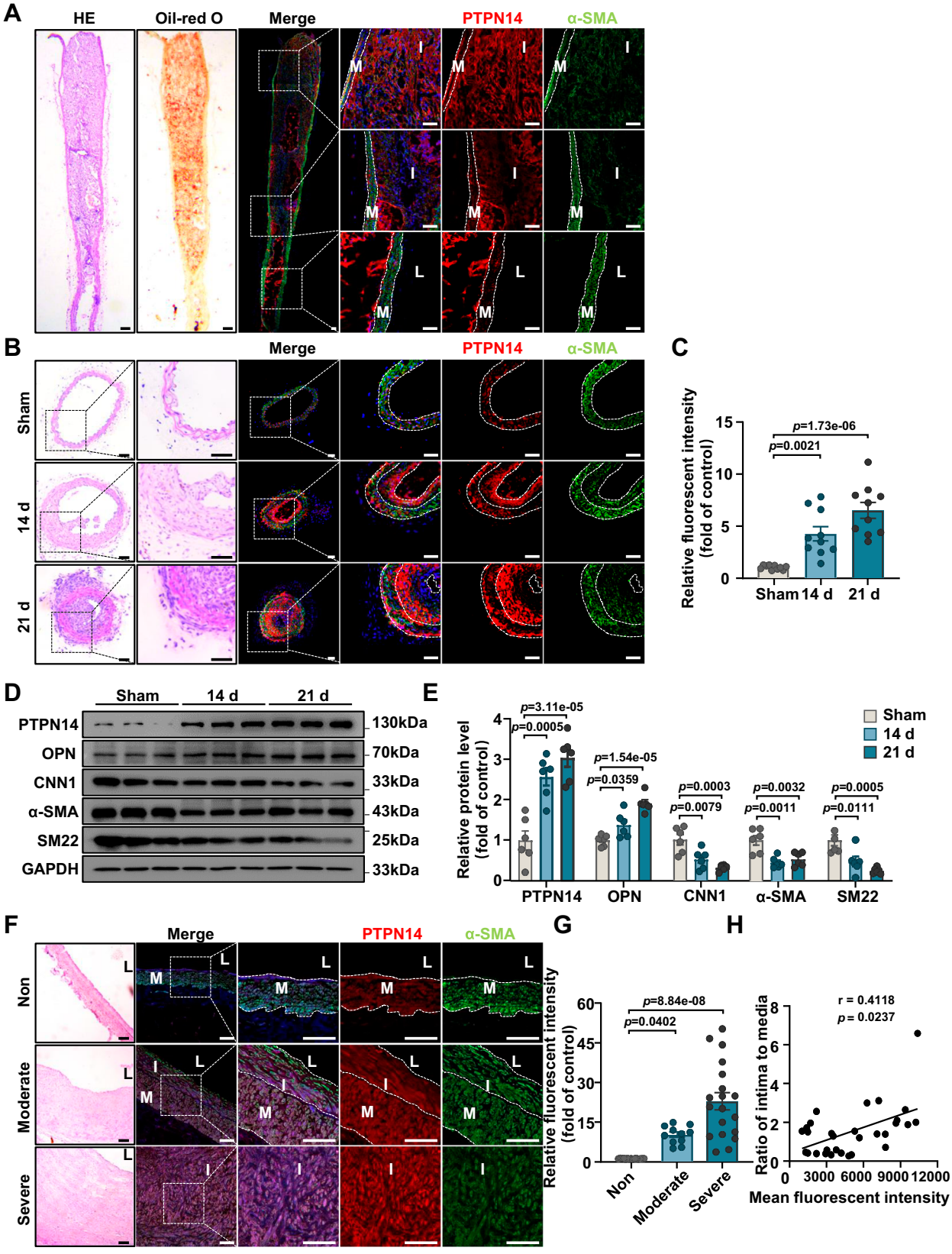

However, PTPN14 overexpression potentiated the effect of PDGF-BB and promoted PDGF-BB-induced VSMC migration, whereas PTPN14^{C1121S} blunted PDGF-BB-induced VSMC migration, as demonstrated in both scratch and Transwell assays (Fig. 3A, D). Furthermore, neither PTPN14 nor PTPN14^{C1121S} overexpression significantly affected VSMC proliferation under basal conditions (Fig. 3E, F). However, overexpression of wild-type PTPN14 increased PDGF-BB-induced VSMC proliferation, as evidenced by an increased number of Ki67-positive cells, while PTPN14^{C1121S} exerted the opposite effect (Fig. 3E, F). Moreover, PTPN14 overexpression promoted PDGF-BB-induced VSMC dedifferentiation, leading to a decrease expression in contractile markers, including α-SMA and SM22, and an increase expression of the

Fig. 1 | PTPN14 expression is induced in VSMCs during neointimal hyperplasia. **A** ApoE$^{-/-}$ mice were subjected to partial ligation of the left carotid artery (LCA) and fed a Western diet for 4 weeks. Representative images of HE, Oil-red O, and immunofluorescence staining of PTPN14 (red) and α-SMA (green) in LCAs. $n = 3$. Nuclei was counterstained with DAPI (blue). Scale bar, 500 μm (HE, Oil-red O), and 50 μm (immunofluorescence). L: Lumen, M: Media, I: Intima. **B** Representative images of HE and immunofluorescence staining from LCAs of C57BL/6 mice at 0, 14, and 21 d after wire injury surgery. PTPN14, red; α-SMA, green; DAPI, blue. Scale bar, 50 μm. **C** Quantification of PTPN14 in the α-SMA-positive area of the LCAs. The data were presented as the means ± SEM, $n = 10$ (one-way ANOVA with Bonferroni multiple comparison post-hoc test). **D**, **E** Western blots and quantification of the expression of PTPN14, OPN, CNN1, α-SMA, and SM22 in LCAs of C57BL/6 mice at 0, 14, and 21 d post-injury. The protein extracts from 2 mice were pooled into 1 sample. The data were presented as the means ± SEM, $n = 6$ (one-way ANOVA with Bonferroni multiple comparison post-hoc test). **F** Representative images of HE and immunofluorescence staining of the human coronary artery. PTPN14, red; α-SMA, green; DAPI, blue. Scale bar, 50 μm. **G** Quantification of the expression of PTPN14 in α-SMA-positive area of human coronary artery. The data were presented as the means ± SEM, $n = 15, 11, 19$, respectively (one-way ANOVA with Bonferroni multiple comparison post-hoc test). **H** The correlation analysis between PTPN14 expression and intima-to-media ratio of human coronary arteries, $n = 30$ (two-tailed non-parametric Spearman correlation). L: Lumen, M: Media, I: Intima.

proliferative marker PCNA and synthetic markers OPN and VIM in HA-VSMCs (Fig. 3G, H). In contrast, PTPN14^{C1121S} overexpression inhibited PDGF-BB-induced VSMC dedifferentiation (Fig. 3G, H), indicating the critical role of PTPN14's phosphatase activity in these processes. In addition, we found that while PTPN14 overexpression did not affect these markers under basal levels, PTPN14^{C1121S} overexpression significantly upregulated the expression of α-SMA and SM22 (Fig. 3G, H). Collectively, these results suggest that PTPN14 promotes PDGF-BB-induced VSMC migration, proliferation, and dedifferentiation, which largely depends on its phosphatase activity.

VSMC-specific PTPN14 deficiency inhibited wire injury-induced neointimal hyperplasia

To elucidate the specific contribution of VSMC-derived PTPN14 to neointimal hyperplasia, we constructed VSMC-specific PTPN14-knockout mice (PTPN14$^{SMC-/-}$) by crossing floxed PTPN14 mice (PTPN14^{flox}) with Tagln-Cre mice (Supplementary Fig. 5A). Immunofluorescence staining of aortas confirmed that the PTPN14 expression was specifically deleted in the VSMCs but not in ECs of vessel in PTPN14$^{SMC-/-}$ mice compared to their littermate controls (PTPN14^{flox}) (Fig. 4A, B). Global PTPN14 knockout in mice has been reported to be associated with lymphatic edema, which occurs in the forelimb, hind limbs, or periorbital area. Additionally, PTPN14 variants cause defects in organ and tissue development in zebrafish embryos[18,19]. However, no obvious phenotypic abnormalities in PTPN14$^{SMC-/-}$ mice were observed until 15 weeks of age, with monitoring discontinued thereafter. Furthermore, there were no morphological differences in the carotid arteries of PTPN14^{flox} and PTPN14$^{SMC-/-}$ mice, as indicated by the comparable mean medial thickness, ratio of medial thickness to lumen size, and ratio of medial thickness to vessel diameter (Supplementary Fig. 5B), suggesting a dispensable role of SMC PTPN14 in vessel development. In addition, VSMC-specific PTPN14 deficiency did not alter the body weight, systolic blood pressure, diastolic blood pressure, mean arterial pressure, or heart rate of mice (Supplementary Fig. 5C).

We subjected both PTPN14^{flox} and PTPN14$^{SMC-/-}$ mice to wire injury to the LCAs for 21 d and found that VSMC-specific PTPN14 deficiency reduced in neointima formation within injured LCAs compared to that in PTPN14^{flox} mice (Fig. 4C). The ratio of intima thickness to lumen size in LCAs at 21 d post-injury, was notably diminished in PTPN14$^{SMC-/-}$ mice compared to that in their PTPN14^{flox} counterparts, while the circumference of the external elastic lamina was comparable between the groups (Fig. 4D). Furthermore, the number of PCNA-positive cells in the intima of the injured LCA was significantly diminished in response to PTPN14 knockout (Fig. 4E, F). To explore the potential sex-related differences in the impact of PTPN14 deficiency on neointima formation, we extended our study to include female PTPN14$^{SMC-/-}$ mice. Consistently, we observed that VSMC-specific PTPN14 deficiency in female mice led to a reduction in neointima formation within injured LCAs compared to that in PTPN14^{flox} mice, as evidenced by a decrease in the ratio of intima thickness to lumen size in the LCAs (Supplementary Fig. 6A, B). In addition, the number of PCNA-positive cells in the intima of injured LCAs was reduced in female PTPN14$^{SMC-/-}$ mice (Supplementary Fig. 6C, D).

Additionally, VSMC-specific PTPN14 deficiency led to a decrease in the expression of the proliferative VSMC marker PCNA, while elevating the levels of contractile VSMC markers, including CNN1, α-SMA, and SM22, in injured LCAs compared to that in littermate PTPN14^{flox} mice (Fig. 4G, H). These results demonstrate that PTPN14 specific deficiency inhibits the loss of the contractile phenotype of VSMCs and wire injury-induced neointimal hyperplasia.

PTPN14 controlled the output of PDGF-BB signaling in VSMCs

We next explored the underlying mechanisms of PTPN14 in phenotypic modulation of VSMCs. HA-VSMCs were transfected with PTPN14 or control siRNA followed by treatment with or without PDGF-BB for 24 h. Subsequently, we performed whole transcriptome analysis using RNA-sequencing of HA-VSMCs (Fig. 5A). As shown in the volcanic map, PTPN14 deficiency resulted in a significant down-regulation of 113 genes and up-regulation of 48 genes in HA-VSMCs, with a threshold of two-fold change and a P value of <0.05 (Fig. 5B). Gene Ontology (GO) analysis followed by network visualization of enriched GO terms using BiNGO indicated that the genes differentially expressed due to PTPN14 deficiency were linked to cell adhesion, growth, differentiation, and migration (Fig. 5C). As the heat map showed that PTPN14 deficiency group displayed a contrasting pattern in the regulation of gene expression when compared with the PDGF-BB-treated group. This led us to speculate that PTPN14 plays a crucial role in PDGF-BB signaling in VSMCs. Next, we performed gene set enrichment analysis (GSEA) using differentially expressed genes after PDGF-BB treatment (563 genes were upregulated and 671 genes were downregulated, compared to PBS treatment). Remarkably, we found that genes that were upregulated upon PDGF-BB stimulation were significantly enriched in the gene sets that were decreased by PTPN14 silencing, while genes that were downregulated upon PDGF-BB stimulation were significantly enriched in the gene sets that were increased by PTPN14 silencing (Fig. 5D), indicating the pivotal role of PTPN14 in the expression of PDGF-BB-induced genes.

We next examined the effects of PTPN14 silencing on the classical downstream signaling initiated by PDGF-BB in VSMCs. We knocked down the expression of PTPN14 in HA-VSMCs using siRNA, and then treated the cells with or without PDGF-BB for up to 30 min. Notably, PTPN14 silencing led to a substantial reduction in the phosphorylation levels of phospholipase C gamma (PLCγ), AKT, and, ERK1/2, all of which are typically induced by PDGF-BB (Fig. 5E, F). Similar results were obtained using another PTPN14 siRNA (Supplementary Fig. 7A, B). To further confirm the necessity of PTPN14 in PDGF-BB-induced SMC migration, proliferation, and differentiation, we conducted prolonged PDGF-BB treatments. Under basal conditions, PTPN14 silencing did not induce any significant alterations in VSMC migration in Transwell assays; however, it impaired VSMC migration in scratch assays at 24 h. Notably, PTPN14 silencing significantly inhibited PDGF-BB-induced VSMC migration, in both scratch and Transwell assays (Supplementary Fig. 8A–D). Furthermore, although PTPN14 silencing did not

https://doi.org/10.1038/s41467-024-51881-x

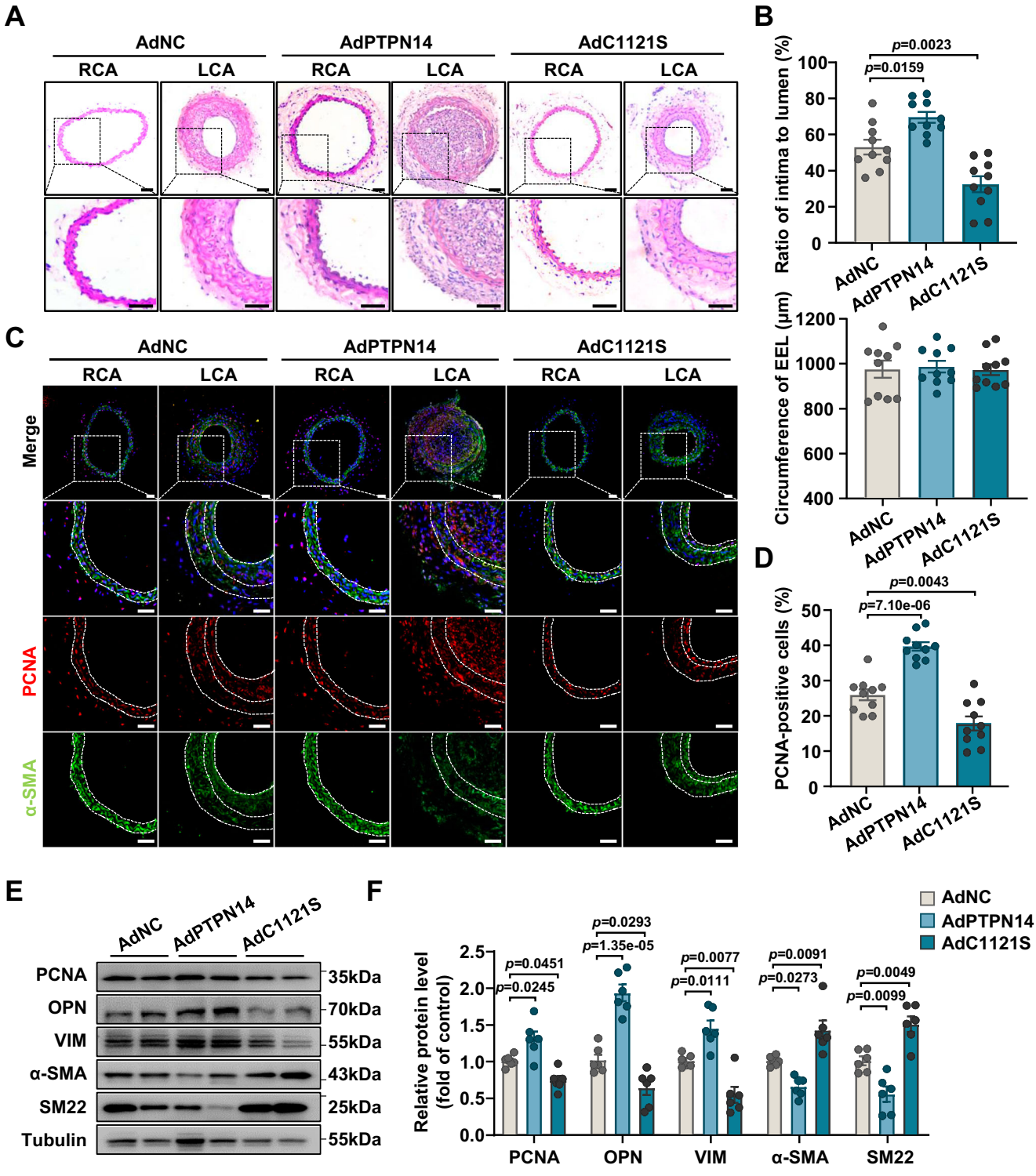

Fig. 2 | PTPN14 aggravates neointimal hyperplasia in a phosphatase activity-dependent manner. C57BL/6 mice subjected to wire injury of left carotid arteries (LCAs) were transfected with AdNC, AdPTPN14, and AdPTPN14^{C1121S} for 14 d. **A** Representative HE staining images of cross-sections from injured LCAs and contralateral uninjured right carotid arteries (RCAs) of mice 14 d after injury. Scale bar, 50 μm. **B** Quantification analysis of the ratios of intima to lumen, and the circumference of external elastic lamina (EEL) in the cross-sections from the LCAs at 14 d post-injury. The data were presented as the means ± SEM, $n = 10$ (one-way ANOVA with Bonferroni multiple comparison post-hoc test). **C**, **D** Representative immunofluorescence staining and quantification of the percentage of PCNA-positive cells in cross-sections of LCAs. PCNA, red; α-SMA, green; DAPI, blue. Scale bar, 50 μm. The data were presented as the means ± SEM, $n = 10$ (one-way ANOVA with Bonferroni multiple comparison post-hoc test). **E**, **F** Western blots and quantification of PCNA, OPN, VIM, α-SMA, and SM22 in LCAs. Protein extracts from 2 mice were pooled into 1 sample. The data were presented as the means ± SEM, $n = 6$ (one-way ANOVA with Bonferroni multiple comparison post-hoc test).

https://doi.org/10.1038/s41467-024-51881-x

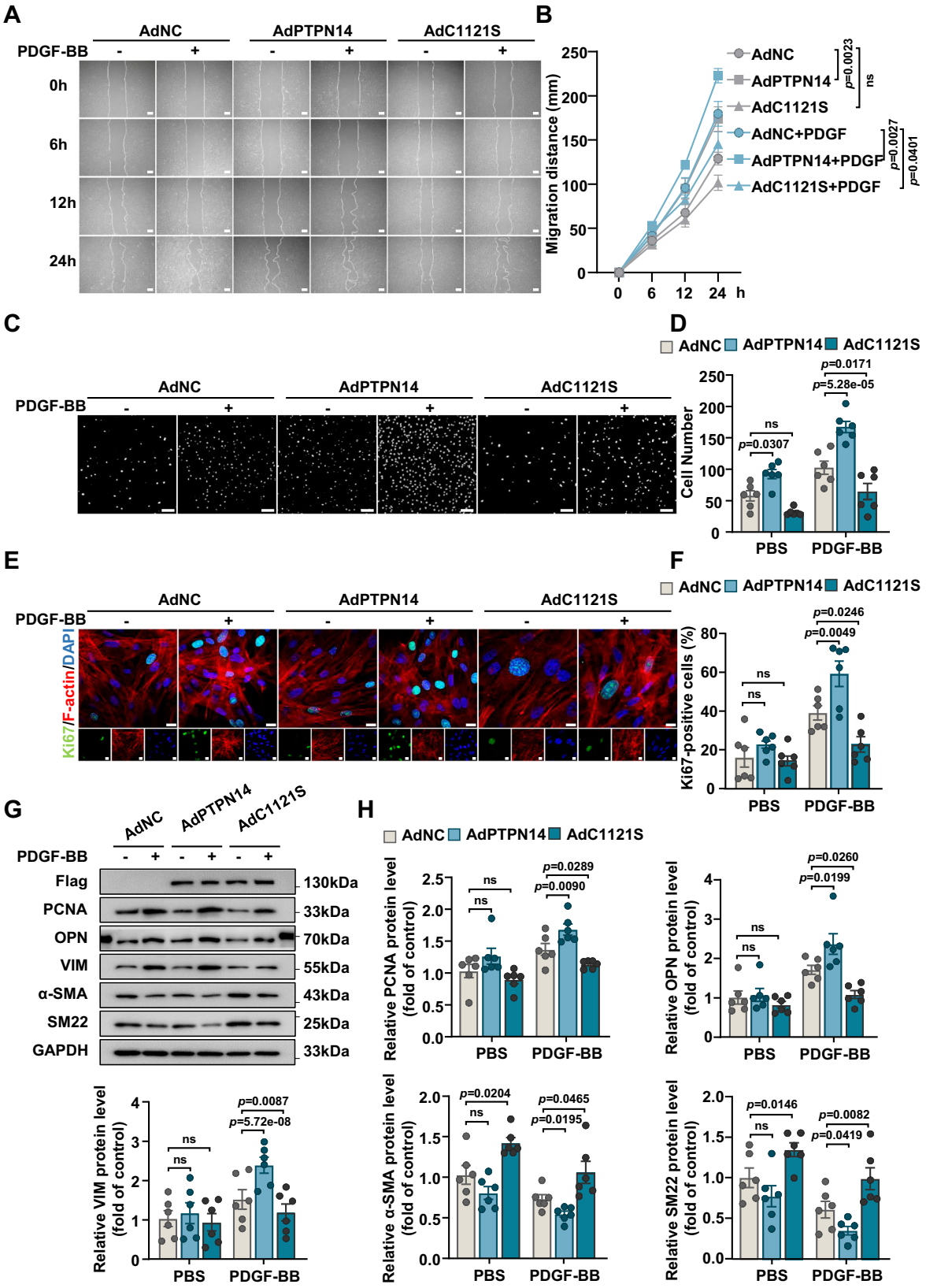

significantly affect the number of Ki67-positive cells under basal conditions, it counteracted the effects of PDGF-BB, resulting in a reduction in the number of Ki67-positive cells (Supplementary Fig. 8E, F). Additionally, while PTPN14 silencing did not significantly impact the expression of the markers including SM22, PCNA, OPN, and VIM, under basal conditions, it significantly upregulated the expression of α-SMA (Fig. 5G, H). Finally, we found that PTPN14 silencing suppressed PDGF-BB-induced VSMC dedifferentiation, as evidenced by an increase in contractile markers, including α-SMA and SM22, along with a decrease in the expression of the proliferative marker PCNA in HA-VSMCs and synthetic markers OPN and VIM (Fig. 5G, H). A similar effect of PTPN14 silencing on VSMC dedifferentiation was observed using

Fig. 3 | PTPN14 promotes PDGF-BB-induced SMC migration, proliferation, and dedifferentiation. Human aortic smooth muscle cells (HA-VSMCs) that underwent FBS-free starvation were transfected with AdNC, AdPTPN14, or AdPTPN14^{C1121S} for 48 h. **A**, **B** Scratch assays were performed on cells with PDGF-BB (20 ng/mL) for the indicated time points. Representative images and quantification were shown. Scale bar, 20 μm. Data were presented as the means ± SEM, $n = 6$ (two-way ANOVA with Bonferroni multiple comparison post-hoc test). **C**, **D** HA-VSMCs treated with PDGF-BB (20 ng/mL) for 6 h were subjected to Transwell assays. Representative images and quantitative analyses were presented. Scale bar, 100 μm. Data were presented as the means ± SEM, $n = 6$ (two-way ANOVA with Bonferroni multiple comparison post-hoc test). **E**, **F** HA-VSMCs were treated with PDGF-BB (20 ng/mL) for 24 h. Representative immunofluorescence staining and quantification of Ki67-positive cells were shown. F-actin, red; Ki67, green; DAPI, blue. Scale bar, 10 μm. Data were presented as the means ± SEM, $n = 6$ (two-way ANOVA with Bonferroni multiple comparison post-hoc test). **G**, **H** Representative western blots and quantification of the protein levels of Flag-tagged PTPN14, PCNA, OPN, VIM, α-SMA, SM22, and GAPDH in the absence or presence of PDGF-BB (20 ng/mL) treatment. The data were presented as the means ± SEM, $n = 6$ (two-way ANOVA with Bonferroni multiple comparison post-hoc test).

another PTPN14 siRNA (Supplementary Fig. 8G, H). These findings suggested that PTPN14 silencing counteracted the effects of PDGF-BB on VSMCs.

PTPN14 interacted with PDGFRβ and mediated its tyrosine dephosphorylation at Y692 site

PDGF-BB served as a ligand of PDGF receptor (PDGFR) isoforms (PDGFRα and PDGFRβ) and its binding with PDGFR results in the activation of multiple downstream signaling pathways[20]. Given the critical role of PTPN14 in mediating PDGF-BB signaling in SMCs, we speculated whether PTPN14 directly interacted with PDGFRα or PDGFRβ. Immunoprecipitation assay indicated that PTPN14 could bind with PDGFRβ but not PDGFRα in HA-VSMCs (Fig. 6A). Besides, we found that PTPN14 and PDGFRβ could interact with each other and the binding was not influenced by PDGF-BB stimulation for 10 min (Fig. 6B). In parallel, we transfected Flag-tagged PTPN14 and HA-tagged PDGFRβ plasmids in HEK293T cells and confirmed the interaction between PTPN14 and PDGFRβ (Fig. 6C, D). Consistently, immunofluorescence staining of PTPN14 and PDGFRβ revealed colocalization signaling (Supplementary Fig. 9A). PDGFRβ comprises a glycosylated immunoglobulin-like extracellular domain, transmembrane region that contributes to membrane localization, and intracellular regions, including juxtamembrane regions and conserved kinase regions that undertake phosphorylation activation functions[21]. To identify which region(s) of PDGFRβ interacts with PTPN14, we expressed multiple HA-tagged PDGFRβ fragments together with full-length Flag-tagged PTPN14 in HEK293T cells. Our findings revealed that the C-terminal region of PDGFRβ (aa 553–1106) but not N-terminal region (aa 1–532) interacted with PTPN14 (Fig. 6E, F). Moreover, PDGFRβ with the deletion of C-terminal (aa 553–1106), but not the deletion of N-terminal (aa 1–532), was incapable of interacting with PTPN14 (Fig. 6E, F). These results suggest that the C-terminal region of PDGFRβ bridge its interaction with PTPN14.

PDGFRβ undergoes receptor dimerization upon PDGF-BB binding, which induces autophosphorylation at the intracellular kinase domain and triggers intracellular Ras-MAPK, phosphoinositide 3-kinase (PI3K)-AKT, Janus kinase, and PLCγ cascade signaling to regulate cell responses[21,22]. As the phosphatase activity of PTPN14 was required for PDGF-BB-induced migration, proliferation, and dedifferentiation of SMCs, we hypothesized that PTPN14 may dephosphorylate PDGFRβ at specific site(s). We overexpressed Myc-tagged PDGFRβ with adenovirus in HA-VSMCs and transfected the cells with PTPN14 or control siRNA. Following the stimulation of PDGF-BB for 10 min, cells from two groups were harvested and the phosphorylation levels of tyrosine sites in PDGFRβ were analyzed using LC-MS/MS (Fig. 6G). Two high-confidence tyrosine phosphorylated sites of PDGFRβ detected via LC-MS/MS showed difference levels in the groups. Of the two sites, only Y692, a tyrosine phosphorylation site of PDGFRβ, exhibited an upregulated phosphorylation level in response to PTPN14 knockdown (Supplementary Table 1). We next confirmed these results using cultured HA-VSMCs. Consistently, we found that PDGF-BB could induce PDGFRβ^{Y692} phosphorylation, which was further enhanced by PTPN14 silencing in HA-VSMCs (Fig. 6H, I). Consistently, similar results were observed using another PTPN14 siRNA (Supplementary Fig. 10A, B). Together, these results demonstrate that PTPN14 interacts with PDGFRβ and promotes the latter's dephosphorylation at Y692 site.

Y692 served as a self-inhibitory phosphorylation site of PDGFRβ

To clarify the role of PDGFRβ^{Y692} phosphorylation on PDGF-BB/PDGFRβ signaling, we constructed phosphomimetic mutant (PDGFRβ^{Y692D}) and phospho-null mutant (PDGFRβ^{Y692F}) of PDGFRβ. We found that neither the mutation impacted the interaction between PDGFRβ and PTPN14 (Supplementary Fig. 11A). However, we found that PDGFRβ^{Y692F} promoted the activation of PDGFRβ downstream targets including AKT and ERK1/2, evidenced by the upregulation of the PDGF-BB-induced phosphorylation (Fig. 7A, B). Conversely, the PDGFRβ^{Y692D} exerted contrasting effects and inhibited PDGF-BB-induced phosphorylation of AKT and ERK1/2 in HA-VSMCs (Fig. 7A, B). Moreover, PTPN14 overexpression upregulated the phosphorylation levels of AKT and ERK1/2 induced by PDGF-BB under PDGFRβ overexpression. However, PTPN14 overexpression had a minimal impact on the phosphorylation levels of AKT and ERK1/2 induced by PDGF-BB following overexpression of either PDGFRβ^{Y692F} or PDGFRβ^{Y692D} in HA-VSMCs (Fig. 7C, D), indicating that the phosphorylation status of PDGFRβ^{Y692} mediates the regulatory effects of PTPN14 on PDGF-BB/PDGFRβ signaling. Consistently, we found that phosphorylation level of PDGFRβ^{Y692} was significantly upregulated in neointima of carotid arteries induced by wire injury in PTPN14$^{SMC-/-}$ mice compared to that in PTPN14^{flox} mice (Fig. 7E, F).

The conformational changes and dimerization of PDGFRβ are required for controlling PDGF-BB-induced PDGFRβ activation[23]. To further investigate the molecular basis of Y692 as an inhibitory phosphorylation site of PDGFRβ, we conducted surface plasmon resonance assay to detect the effects of Y692 phos-mutant on the binding affinity of PDGF-BB and PDGFRβ. We found that compared to wild-type PDGFRβ, phosphomimetic mutant of PDGFRβ displayed an upregulation in K_D value of interaction with PDGF-BB compared to that in wild-type PDGFRβ (Fig. 7G). However, this PDGFRβ mutation had minimal effects on its interaction with PDGF-DD, as the binding affinity remained unaltered (Supplementary Fig. 12A). Furthermore, in situ proximity ligation assay staining of PDGF-BB and PDGFRβ in LCAs 21 d post-wire injury indicated that the interaction was compromised by PTPN14 deficiency (Fig. 7H, I). Moreover, we observed that PDGFRβ^{Y692F} promoted, while PDGFRβ^{Y692D} attenuated PDGF-BB-induced PDGFRβ dimerization in HA-VSMCs (Fig. 7J). Together, the results indicated that Y692 served as a self-inhibitory phosphorylation site of PDGFRβ via controlling its binding with PDGF-BB and dimerization.

PTPN14 aggravated neointimal hyperplasia by dephosphorylating PDGFRβ^{Y692}

We next investigated the effects of PDGFRβ^{Y692} on PDGF-BB-induced migration, proliferation, and dedifferentiation of VSMCs. We found that PDGFRβ^{Y692F} had minimal effects on VSMC migration and proliferation in basal level, while it markedly enhanced these processes under PDGF-BB treatment (Fig. 8A–C and Supplementary Fig. 13A–C). Conversely, PDGFRβ^{Y692D} inhibited the migration and proliferation of VSMCs regardless of the presence of PDGF-BB (Fig. 8A–C and Supplementary Fig. 13A–C). To further elucidate the role of PDGFRβ^{Y692}

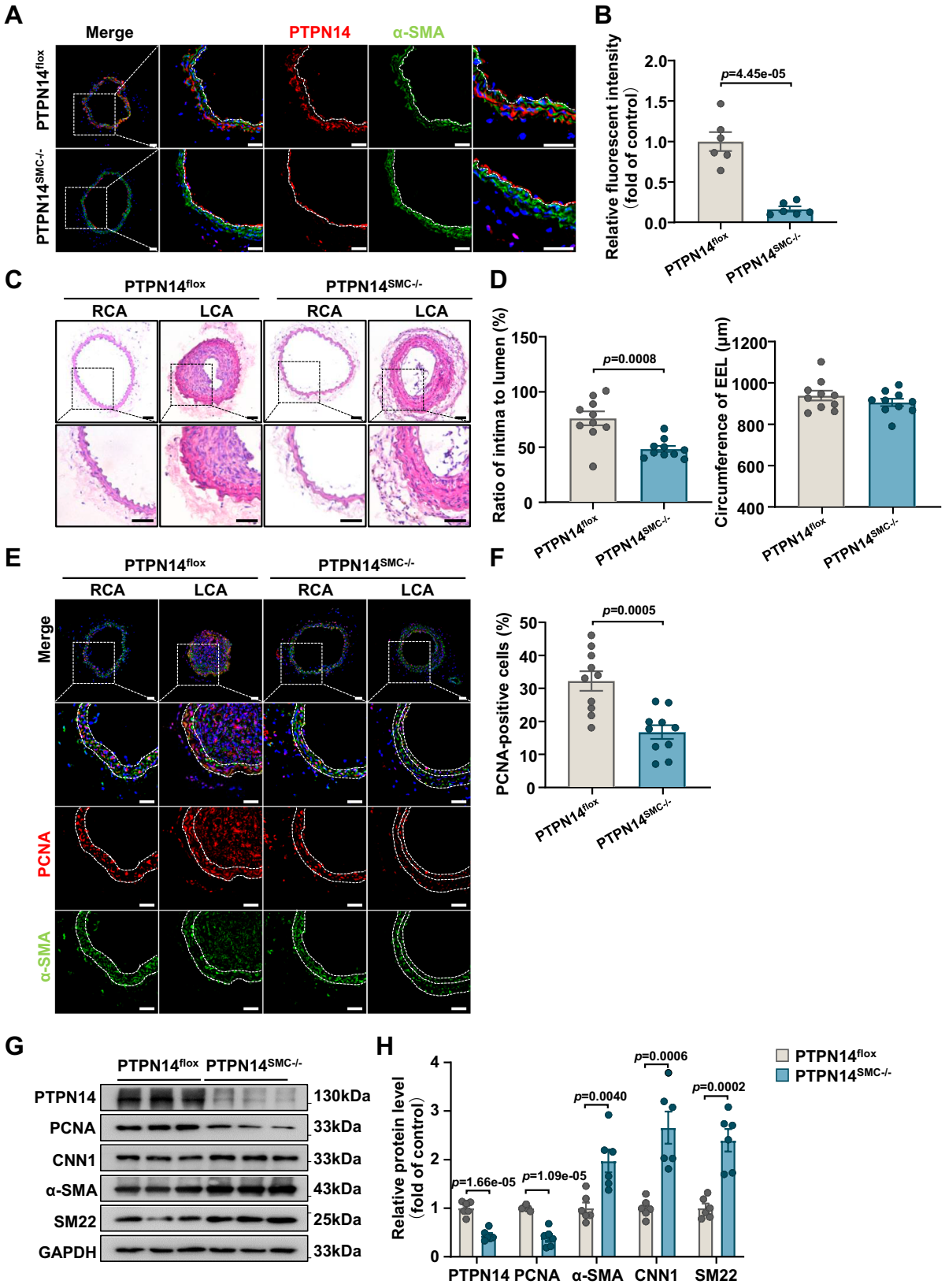

phosphorylation in wire injure-induced neointimal hyperplasia and its correlation with PTPN14, we constructed adenovirus carrying PDGFRβ^{Y692F} (AdPDGFRβ^{Y692F}) and PDGFRβ^{Y692D} (AdPDGFRβ^{Y692D}), and further overexpressed the mutants in wire-injured carotid arteries of PTPN14$^{SMC-/-}$ and PTPN14^{flox} mice (Supplementary Fig. 13D). Consistent with the in vitro results, we found that forced expression of PDGFRβ^{Y692F} promoted neointima formation and increased the number of proliferating PCNA-positive cells in LCAs 14 d post-injury in PTPN14^{flox} mice (Fig. 8D–G). Notably, PDGFRβ^{Y692F} overexpression largely antagonized the effects of PTPN14 deficiency on wire injury-induced neointima formation in LCAs (Fig. 8D–G). Moreover, we found that PDGFRβ^{Y692D} overexpression recapitulated the effects of PTPN14

Fig. 4 | VSMC-specific PTPN14 deficiency inhibits wire injury-induced neointimal hyperplasia. A Representative immunofluorescence staining of PTPN14 and α-SMA in the right carotid arteries (RCAs) from PTPN14 $^{SMC-/-}$ and PTPN14^{flox} mice. PTPN14, red; α-SMA, green; DAPI, blue. Scale bar, 50 μm. The white dashed line signifies the internal elastic lamina. **B** Quantification of PTPN14 in RCAs showed the efficiency on knock out PTPN14. The data were presented as the means ± SEM, $n = 6$ (two-tailed unpaired Student's t test). **C**–**H** VSMC-specific PTPN14 deficiency mice (PTPN14$^{SMC-/-}$) and the littermate control mice (PTPN14^{flox}) were subjected to wire injury of left carotid arteries (LCAs) for 21 d. **C** Representative HE staining images of cross-sections of LCAs and contralateral uninjured RCAs in PTPN14$^{SMC-/-}$ and PTPN14^{flox} mice. Scale bar, 50 μm. **D** Quantification analysis of the ratios of intima to lumen, and the circumference of external elastic lamina (EEL) of the cross-sections of LCAs. The data were presented as the means ± SEM, $n = 10$ (two-tailed unpaired Student's t test). **E**, **F** Representative immunofluorescence staining of PCNA and α-SMA in the cross-sections of LCAs and RCAs. Quantification of PCNA-positive cells in the LCAs. PCNA, red; α-SMA, green; DAPI, blue. Scale bar, 50 μm. The data were presented as the means ± SEM, $n = 10$ (two-tailed unpaired Student's t test). **G**, **H** Representative western blots and quantification of the protein level of PTPN14, PCNA, CNN1, α-SMA, SM22, and GAPDH in LCAs. Protein extracts from 2 mice were pooled into 1 sample. The data were presented as the mean ± SEM, $n = 6$ (two-tailed unpaired Student's t test).

deficiency with alleviating wire injure-induced neointimal hyperplasia and reducing PCNA-positive cells in LCAs of PTPN14^{flox} mice (Fig. 8D–G). No synergetic effects between PTPN14 deficiency and PDGFRβ^{Y692D} overexpression was observed (Fig. 8D–G). In addition, either PDGFRβ^{Y692F} or PDGFRβ^{Y692D} barely affected the circumference of the external elastic lamina (Fig. 8D, E). We further confirmed the potential link between PDGFRβ^{Y692} phosphorylation and neointimal hyperplasia in human coronary arteries. Indeed, we found that phosphorylation levels of PDGFRβ^{Y692} were lower in neointima of moderate and severe hyperplasia group compared to that of non-hyperplasia group (Fig. 8H, I). Besides, the levels of phosphorylated PDGFRβ^{Y692} were negatively correlated to the ratios of intima to media (Fig. 8J). Therefore, these results suggest that PDGFRβ^{Y692} phosphorylation in VSMCs alleviates wire injury-induced neointimal hyperplasia and mediates the effects of PTPN14 deficiency on neointima formation.

Discussion

Despite decades of research and numerous clinical trials, neointimal hyperplasia and the subsequent restenosis remain challenging clinical problems. Herein, we demonstrated that PTPN14, which is enriched in VSMCs within neointimal hyperplasia and induced by PDGF-BB, plays a role in migration, proliferation, and dedifferentiation of VSMCs and aggravates wire injury-induced neointimal hyperplasia in mice, presenting a positive-feedback loop in boosting PDGF-BB/PDGFRβ signaling. Previous studies have highlighted the vital role of PDGF-BB/PDGFRβ signaling in facilitating dedifferentiation of VSMCs and subsequent neointima formation. We revealed that phosphorylation of PDGFRβ^{Y692}, which can be dephosphorylated by PTPN14, acts as a restrictive element governing intracellular outputs of PDGFRβ activation, including PLCγ, AKT, and ERK1/2, and serves as an endogenous self-inhibitory signaling of PDGFRβ (Fig. 9). Hence, the present study suggests a potential role for the PTPN14/PDGFRβ^{Y692} signaling axis in neointimal hyperplasia, which might shed light on the therapeutic strategy for atherosclerosis and restenosis.

Tyrosine phosphorylation regulates many cellular functions, including cell proliferation, survival, adhesion, and migration[24,25]. Members of the protein tyrosine phosphatase (PTP) family orchestrate the state of tyrosine phosphorylation through removing phosphate from the substrates. According to the subcellular location, classical PTPs (38 members), which show specificity for phosphotyrosine, can be divided into non-receptor PTPs (PTPNs, 17 members) and transmembrane receptor PTPs (RPTPs, 21 members)[26]. In contrast to RPTPs, which usually contain two catalytic domains[27], PTPNs encode a single PTP domain that executes nucleophilic attacks on their phosphosubstrates. Multiple PTPNs are involved in VSMC phenotypic modulation and neointimal hyperplasia. Similar to the expression pattern of PTPN14, PTPN1 (also known as PTP1B) expression can be induced in VSMCs by PDGF-BB, both in vitro and in rat carotid arteries after injury[28]. However, PTPN1 dephosphorylates several receptor tyrosine kinases (RTKs), including EGFR and PDGFR, and inhibits PDGF-BB-induced proliferation and motility of VSMCs[29]. PTPN6 (also known as SHP-1) overexpression inhibits the proliferation, cell cycle progression, and migration of VSMCs and reduces neointima formation induced by wire injury in the femoral arteries of high-fat diet-fed mice[30]. PTPN11 expression can be transiently induced in neointima of rat carotid arteries after injury, and growth factors, including PDGF and bFGF, are sufficient to induce its expression in VSMCs[28]. Inducible VSMC-specific deletion of PTPN11 in adult mice suppresses carotid artery ligation-induced neointima formation by attenuating VSMC proliferation and decreasing ECM[31]. Despite these findings, PTPN14 is uncharacterized and its role in VSMCs remains elusive. In the present study, we observed that PTPN14 expression in VSMCs robustly induced during phenotypic modulation in the carotid arteries from three distinct mouse models and in human coronary arteries. In addition, we demonstrated that PTPN14 expression positively correlated with the degree of hyperplasia in human samples, indicating its potential role as a biomarker of restenosis. Furthermore, we found that VSMC-specific PTPN14 deficiency was suppressed, whereas overexpression of PTPN14 promoted neointima formation in the mouse carotid artery induced by wire injury. The distinct structures of PTPNs may contribute to their differential appearance in VSMCs. Although the core catalytic sequences of the PTP domain in the C-terminus are relatively conserved in PTPNs, PTPN14 contains the N-terminal conserved FERM domain[32]. FERM domain is responsible for targeting cytoskeletal proteins to the membrane-cytoskeleton interface and is lacking in PTPN1, PTPN6, and PTPN11. Of note, as PTPN14 exerted its pro-proliferative effects by enhancing PDGF-BB/PDGFRβ signaling pathway and PTPN14 protein levels were induced during VSMC phenotypic modulation or by prolonged exposure to PDGF-BB in VSMCs, we demonstrated a positive-feedback mechanism for neointima formation.

Although the role of PTPN14 in vascular biology is largely unknown, it has been shown to be critical in regulating proliferation and apoptosis in tumor cells and to function as a tumor suppressor. We previously found that endothelial PTPN14 deletion resulted in inflammatory effects and promoted disturbed flow-induced atherosclerosis in the LCAs of mice[12]. In contrast, mice with a specific deletion of PTPN14 in VSMCs showed suppressed neointima formation, which might potentially ameliorate atherosclerosis, indicating that PTPN14 in ECs and VSMCs exerts divergent effects on atherosclerosis. Several factors may have contributed to this observation, including the relatively low baseline expression of PTPN14 in quiescent VSMCs, as illustrated in Fig. 1A, where we observed markedly lower PTPN14 expression in VSMCs than in ECs. Furthermore PTPN14 has shown promising effects on inhibiting the activation of YAP, a critical downstream transcriptional co-activator of the Hippo signaling pathway that regulates cell survival, proliferation, organ development[33,34]. PTPN14 binds to the WW domain of YAP via its PPxY domain and promotes YAP retention in the cytoplasm to suppress tumor cell proliferation and turnover[35–37]. In addition, PTPN14 can bind to Kibra to activate LAST1, resulting in reduced YAP/TAZ localization in the nucleus[38,39]. YAP expression was enhanced by PDGF-BB in vitro and was markedly upregulated in injured vessels[40]. Nuclear localization of YAP is increased in balloon-injured carotid arteries, indicating that YAP is activated during VSMC phenotypic modulation[41]. YAP also promotes the proliferation, migration, and dedifferentiation of VSMCs and aggravates neointima formation[40–42]. We previously demonstrated that

endothelial PTPN14 overexpression reduces disturbed flow-induced YAP phosphorylation at Y357 and exerts its effect in a YAP-dependent manner[12]. In this study, we used an inactivating mutant of PTPN14, PTPN14^{C1121S}, in a series of in vitro and in vivo experiments to demonstrate that the proliferative effects of PTPN14 depend on its phosphatase activity. Nevertheless, given that our previous findings indicated significantly lower YAP^{Y357} phosphorylation in VSMCs than in ECs, it is plausible that PTPN14 may preferentially target alternative substrates in VSMCs. Therefore, the involvement of YAP and fine-tuning of substrate selection of PTPN14 warrant further investigation.

Previous studies have identified several PTPN14 substrates including p130Cas, RIN1, PKC-δ, β-catenin, Roquin2, Caveolin-1, and

Fig. 5 | PTPN14 controls the output of PDGF-BB signaling in VSMCs. Human aortic smooth muscle cells (HA-VSMCs) were transfected with control (siNC) or PTPN14 (siPTPN14) small interfering RNA for 48 h, following the treatment of PDGF-BB (20 ng/mL) or PBS control for 24 h. **A** Heatmap comparison of differentially expression genes among the indicated treatment groups. **B** The volcano map showed upregulated or downregulated differentially expresses genes induced by PTPN14 knockdown. **C** The cytoscape visualization of GO molecular function was performed for differentially expressed genes regulated by PTPN14 knockdown. **D** The GSEA enrichment profile showed the enrichment of differentially expressed genes stimulated by PDGF-BB (20 ng/mL) in siPTPN14 vs. siNC (two-tailed permutation test). **E**, **F** HA-VSMCs were harvested after stimulation with PDGF-BB (10 ng/mL) for 0, 10, and 30 min. Western blots and quantification of the indicated proteins were performed. The data were presented as the means ± SEM, $n = 6$ (two-way ANOVA with Bonferroni multiple comparison post-hoc test). **G**, **H** Representative western blots and quantification of the indicated protein levels in the presence or absence of PDGF-BB (20 ng/mL) treatment for 24 h. The data were presented as the means ± SEM, $n = 6$ (two-way ANOVA with Bonferroni multiple comparison post-hoc test).

VE-cadherin[9,14,15,43–45]. P130Cas is a direct substrate of PTPN14, which specifically regulates the phosphorylation of p130Cas at Y128 in colorectal cancer cells[44]. PTPN14 reduces the phosphorylation of RIN1 at Y36 and of PRKCD at Y374 to regulate cell metastasis by restricting the transport of membrane-bound proteins[9,46]. Dephosphorylation of β-catenin by PTPN14 can reduce the cell-cell adhesion to inhibit the cell migration[43]. PTPN14 mediates the dephosphorylation of Roquin2 at Y691 and promotes the degradation of Roquin2 protein in a KLHL6-dependent manner[45]. PTPN14 dephosphorylates caveolin-1 at Y14, which weakens cell metastasis[15]. In addition, PLD2 promotes PTPN14-mediated dephosphorylation of VE-cadherin to restore the endothelial barrier[14]. In the present study, we observed an interaction between PTPN14 and PDGFRβ in VSMCs. Both mass spectrometry analysis and western blot assays demonstrated that PTPN14 silencing increased the phosphorylation level of PDGFRβ at Y692 site. Moreover, VSMC-specific PTPN14 deletion upregulates the phosphorylation level of PDGFRβ^{Y692} in neointima of injured carotid arteries. Hence, our results suggest that PDGFRβ represents a substrate of PTPN14, with PTPN14 acting to dephosphorylate PDGFRβ^{Y692} in VSMCs. It's important to note that the crystal structure of PTPN14 protein remains elusive, and further structural investigations will provide more insights into the interaction between PTPN14 and PDGFRβ. The PDGFR family, belonging to class III subtype of RTKs, comprises PDGFRα and PDGFRβ. Two PDGFRs dimerize upon binding to ligands, resulting in the formation of PDGFRα homodimers, PDGFRα/β heterodimers, or PDGFRβ homodimers. We found that PTPN14 could not bind to PDGFRα in VSMCs, indicating that PDGFRβ might be the predominant targeted mitogen receptor of PTPN14 in VSMCs. Additionally, PDGFRα and PDGFRβ have an amino acid similarity of 31%, 85%, and 75% in the extracellular, the N-terminal kinase, and C-terminal kinase domains, respectively[47]. Our results indicate that the intracellular kinase domain of PDGFRβ bridges its interaction with PTPN14. The distinct amino acid sequence compositions of the receptors may have contributed to the differences in the interaction patterns. Additionally, we found that PTPN14 overexpression enhanced, whereas PTPN14 silencing inhibited VSMC migration in the absence of PDGF-BB. Besides, PTPN14^{C1121S} overexpression upregulated the expression of α-SMA and SM22, while PTPN14 silencing reduced the expression of α-SMA, under basal conditions. Hence, our results indicate that PTPN14 may also exert PDGFRβ-independent roles in regulating VSMC migration and dedifferentiation.

After PDGF binding and dimerization, autophosphorylation occurs on multiple tyrosine residues within the intracellular domains of PDGFRβ due to the close proximity of the two kinase domains following dimerization and/or its conformational change[22,23]. For instance, phosphorylation of PDGFRβ at Y857 is the primary autophosphorylation site and initiates extensive autophosphorylation of other tyrosine residues. These phosphorylated tyrosine residues further provide docking sites for the downstream signal transduction molecules[48,49]. Specifically, Y751 and Y740 of PDGFRβ act as docking sites for PI3K; Y771 serves as a docking site for GAP, while Y1009 and Y1021 act as docking sites for PLCγ[50–53]. Our LC-MS/MS analysis identified two phosphorylation sites of PDGFRβ, Y751 and Y692, which are regulated by PTPN14 deficiency. Although we demonstrated that PTPN14-mediated dephosphorylation of PDGFRβ at Y692 contributed to VSMC phenotypic modulation and neointima formation, the potential involvement and regulatory mechanism of Y751 of PDGFRβ by PTPN14 remain unknown. Furthermore, we found that the phosphorylation of PDGFRβ at Y692 site was under detectable level in quiescent HA-VSMCs, while it could be detected with a relative low level in non-hyperplasia vessels. Additionally, the phosphorylation of PDGFRβ^{Y692} could be induced by PDGF-BB treatment in VSMCs and further elevated by PTPN14 silencing. However, the precise mechanism underlying the PDGF-BB-induced phosphorylation of PDGFRβ^{Y692} remains elusive. Further investigations are warranted to determine whether this site represents a novel autophosphorylation site or whether alternative phosphorylation mechanisms are involved. PDGFRβ also displays other self-inhibition mechanisms. A glutamic acid/proline repeat motif in the C-terminal tail and a valine in the cytoplasmic juxtamembrane domain of PDGFRβ display self-inhibitory roles for the receptor in the absence of ligand binding[54,55]. Here, we present evidence that PDGFRβ^{Y692} may represent another self-inhibitory mechanism for the activation of the PDGF-BB-induced PDGFRβ signaling pathway. Through gain- and loss-of-function experiments, we demonstrated that the constitutive activation of PDGFRβ^{Y692} significantly attenuated PDGF-BB-induced PDGFRβ signaling pathway activation, while the dominant negative mutant of PDGFRβ^{Y692} exerted the opposite effects. Importantly, PDGFRβ^{Y692} constitutive activation markedly ameliorates wire injury-induced neointima formation, whereas the PDGFRβ^{Y692} dominant negative mutant blunts the effects of PTPN14 deficiency on neointima formation, indicating that targeting PDGFRβ^{Y692} might be a therapeutic strategy for neointimal hyperplasia. Moreover, we observed that PDGFRβ^{Y692} constitutive activation reduced its binding affinity to PDGF-BB and inhibited PDGF-BB-induced PDGFRβ dimerization, indicating that the inhibitory effects might depend on the conformational change of PDGFRβ.

In conclusion, our results demonstrate that PTPN14 is a critical mediator of neointima formation. We elucidated that PTPN14 interacts with PDGFRβ and mediates the dephosphorylation of PDGFRβ at Y692 in VSMCs, thereby enhancing the activation of PDGF-BB/PDGFRβ signaling and aggravating neointimal hyperplasia. Moreover, we identified PDGFRβ^{Y692} as a self-inhibitory site of PDGFRβ signaling cascade, presenting an appealing target for neointimal hyperplasia.

Methods

Animals

The investigation conformed to the Guide for the Care and Use of Laboratory Animals by the US National Institutes of Health (NIH Publication No. 85-23, revised in 2011). Study protocols and the use of animals involved were approved by Institutional Animal Care and Use Committee of Tianjin Medical University. The 8-week-old male ApoE$^{-/-}$ mice and 8- to 12-week-old male wild-type C57BL/6 were purchased from the Experimental Animal Centre of Military Medical Science Academy (Beijing, China). The PTPN14^{flox} mice (Strain NO. T020775) were generated from GemPharmatech (Nanjing, China). The Tagln-Cre mice (Strain NO. 017491) were obtained from MODEL ORGANISMS (Shanghai, China). Tagln-Cre-mediated PTPN14 knockout mice

https://doi.org/10.1038/s41467-024-51881-x

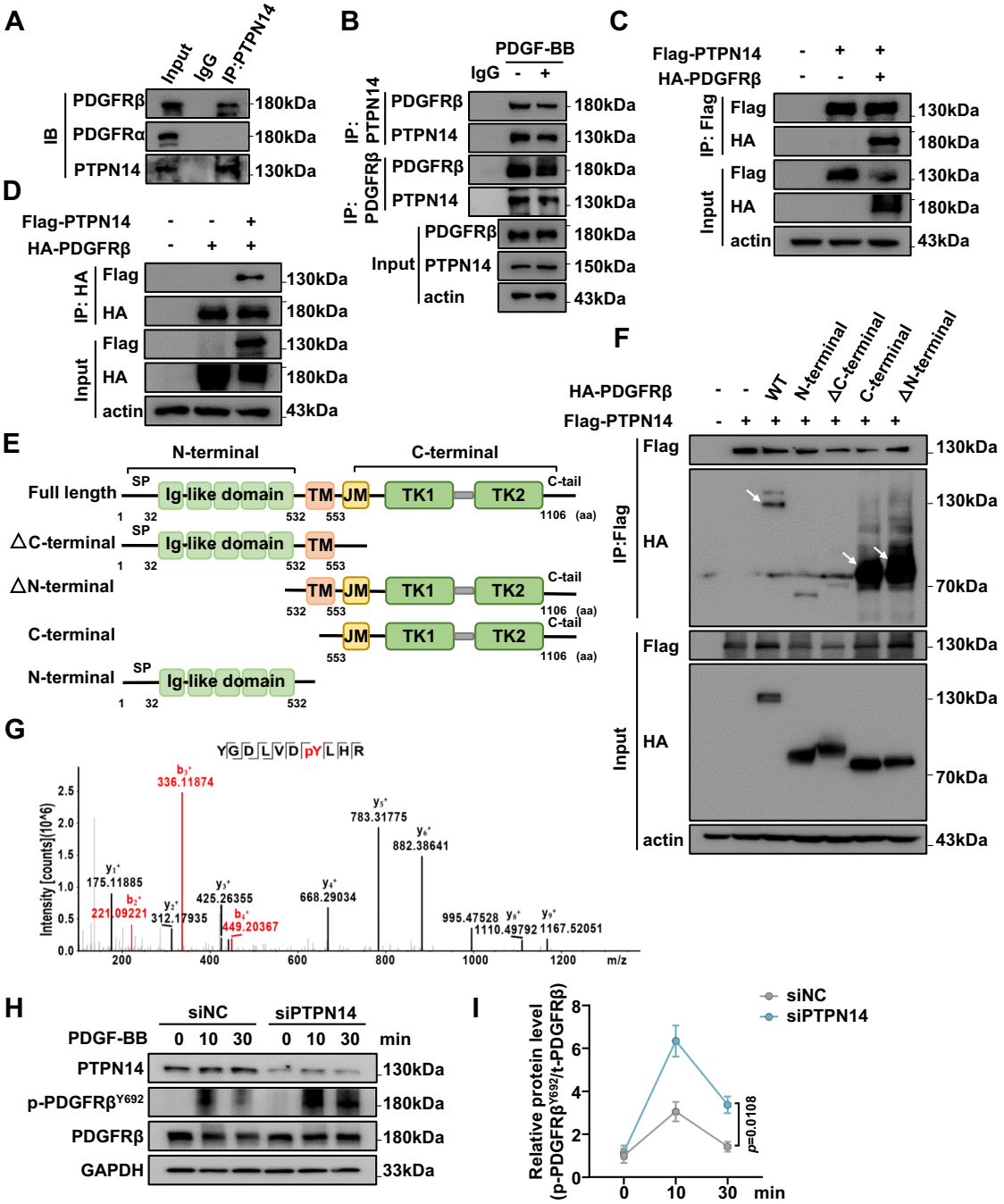

Fig. 6 | PTPN14 interacted with PDGFRβ and mediated its dephosphorylation at Y692 site. A Representative western blots of PDGFRs immunoprecipitated using PTPN14 antibody in human aortic smooth muscle cells (HA-VSMCs). $n = 3$. **B** HA-VSMCs were treated with PDGF-BB (20 ng/mL) or the PBS control for 10 min. Confirmation of the interaction between PDGFRβ and PTPN14 via western blot analysis. $n = 3$. **C**, **D** The co-immunoprecipitation assay to confirm the interaction with co-transfected Flag-tagged PTPN14 (Flag-PTPN14) and HA-tagged PDGFRβ (HA-PDGFRβ) in HEK293T. $n = 3$. **E** Schematic diagram of plasmid truncations construction of PDGFRβ. The positions of the amino acid residues of each structural domain were labeled. **F** The immunoprecipitation assay was performed to detect the interaction among PTPN14 and various domain fragments of PDGFRβ with Flag-PTPN14 and HA-PDGFRβ domains in HEK293T. $n = 3$. **G** HA-VSMCs were transfected with control (siNC) or PTPN14 (siPTPN14) small interfering RNA, then treated with adenovirus to overexpress PDGFRβ for 48 h. After stimulation with PDGF-BB (10 ng/mL) for 10 min, cells were harvested for phosphorylation site detection. Mass spectrometry analysis profile of PDGFRβ dephosphorylated by PTPN14 at Y692. $n = 3$. **H**–**I** HA-VSMCs were transfected with siNC or siPTPN14, then treated with PDGF-BB (10 ng/mL) for indicated time. Representative western blots and quantification of PDGFRβ phosphorylation level at Y692. The data were presented as the means ± SEM, $n = 6$ (two-way ANOVA with Bonferroni multiple comparison post-hoc test).

(PTPN14$^{SMC-/-}$) were generated by crossbreeding PTPN14^{flox} mice with Tagln-Cre mice. All mice were fed a standard chow diet, except for ApoE$^{-/-}$ mice, which were fed a Western diet (Research Diets, Cat NO. D12109C) containing 40 kcal% fat, 1.25% cholesterol, and 0.5% cholic acid after partial ligation for 4 weeks. The mice were bred at 20–26 °C temperature with a 12 h light and12 h dark cycle. Male mice were used in most of the experiments, and some experiments were validated using female mice.

https://doi.org/10.1038/s41467-024-51881-x

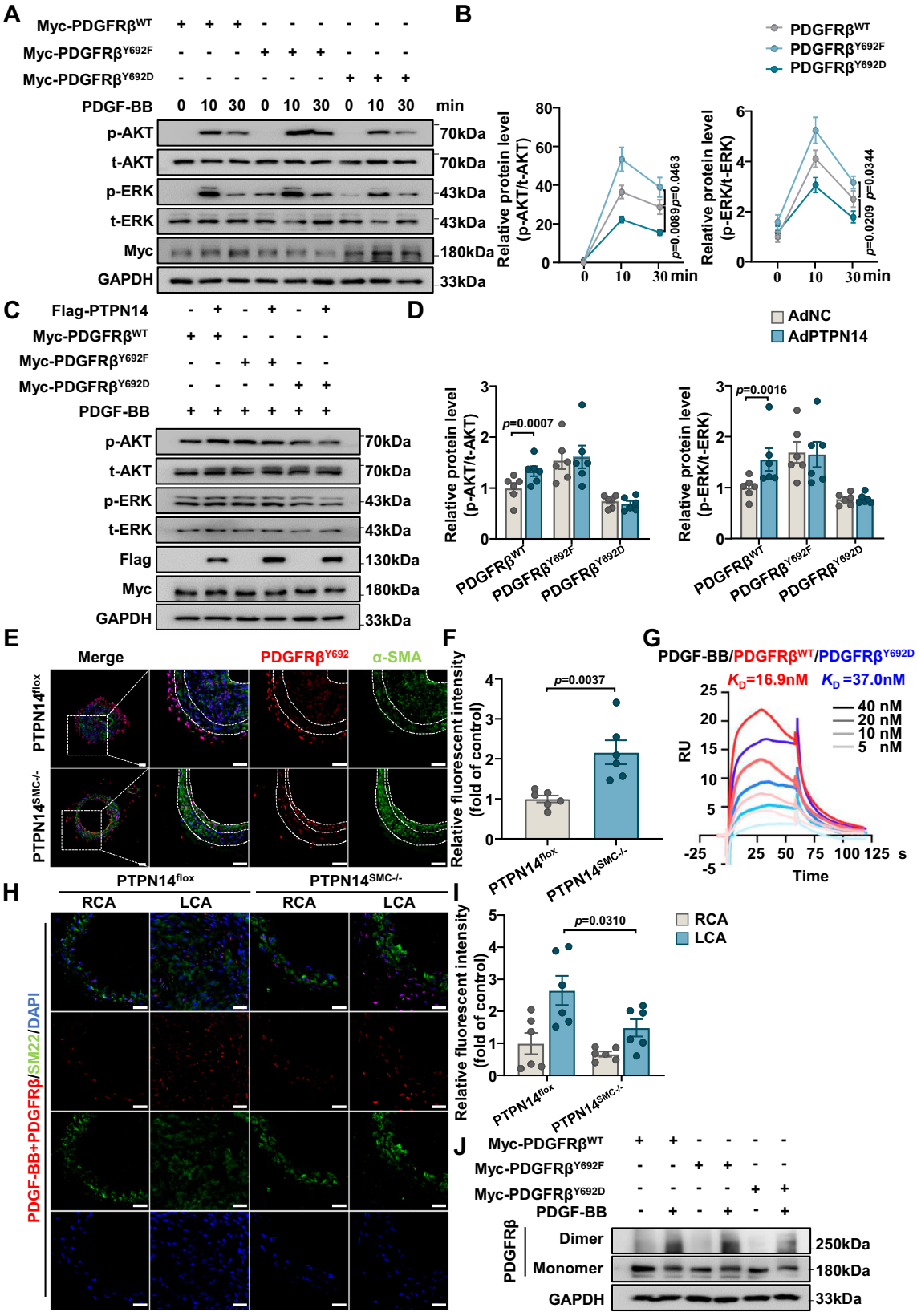

Mouse carotid artery wire injury

After anesthesia, a median incision in the neck of mice was performed. The connective tissue and adipose tissue were bluntly separated to locate LCA and its bifurcation. The clamp temporarily clamped the common carotid artery and the internal carotid artery to stop blood flow. The distal end of the external carotid artery was ligated with a suture to block blood return. Then, LCA was injured by inserting the guide wire below the ligation point. After the guide wire (0.38 mm) was moved back and forth for 5 times, the guide wire was removed and ligation was performed at the proximal end of the external carotid artery. Normal arterial flow was observed and the neck incision was sutured. 14 or 21 d after injury, the arteries were harvested. The arteries

Fig. 7 | Y692 served as a self-inhibitory phosphorylation site of PDGFRβ. **A**, **B** Human aortic smooth muscle cells (HA-VSMCs) were transfected with indicated adenovirus for 48 h, followed by PDGF-BB (10 ng/mL) stimulation for 0, 10, and 30 min. Representative western blots and quantifications of the expression level of indicated proteins. The data were presented as the means ± SEM, $n = 6$ (two-way ANOVA with Bonferroni multiple comparison post-hoc test). **C**, **D** HA-VSMCs were transfected with indicated adenovirus for 48 h, followed by stimulation with PDGF-BB (10 ng/mL) for 10 min. Representative western blots and quantification of the expression level of indicated proteins. The data were presented as the means ± SEM, $n = 6$ (two-way ANOVA with Bonferroni multiple comparison post-hoc test). **E**, **F** PTPN14$^{SMC-/-}$ and the littermate PTPN14^{flox} mice were subjected to wire injury of the left carotid arteries (LCAs) for 21 d. Representative immunofluorescence staining of phosphor-PDGFRβ^{Y692} and α-SMA in cross-sections of the LCAs. Quantification of the levels of phosphor-PDGFRβ^{Y692}. PDGFRβ^{Y692}, red; α-SMA, green; DAPI, blue. Scale bar, 50 μm. The data were presented as the means ± SEM, $n = 6$ (two-tailed unpaired Student's t test). **G** The binding affinity of PDGF-BB to recombinant protein PDGFRβ and PDGFRβ^{Y692D} were measured via surface plasmon resonance. **H**, **I** Representative immunofluorescence staining of in situ proximity ligation assay for visualization on the interaction between PDGF-BB and PDGFRβ in right carotid arteries (RCAs) and LCAs of PTPN14$^{SMC-/-}$ and PTPN14^{flox} mice 21 d post-injury, respectively. Positive signal of PDGF-BB and PDGFRβ, red; SM22, green; DAPI, blue. Scale bar, 20 μm. Quantification of the positive signal (red) in cross-sections of the RCAs and LCAs. The data were presented as the means ± SEM, $n = 6$ (two-way ANOVA with Bonferroni multiple comparison post-hoc test). **J** HA-VSMCs were transfected with the indicated adenoviruses for 48 h, followed by stimulation with PDGF-BB (50 ng/mL) for 30 min. Cells were then incubated with disuccinimidyl suberate (100 μM) at room temperature for 30 min. Representative western blots images of PDGFRβ dimerization were presented, $n = 3$.

were embedded in Tissue Tek OCT compound (Sakura Finetek, Staufen, Germany) for immunofluorescence and morphological staining; the arteries were frozen for western blot and real-time quantitative PCR. The right carotid arteries (RCAs) were used as sham operation group. For adenovirus overexpression experiments, a single dose of 5×10^9 plaque-forming units (pfu) of adenovirus dissolved in 30% pluronic gel solution (Pluronic® F-127, Sigma-Aldrich, St. Louis, MO, USA) was perivascularly delivered to LCAs and RCAs before closing the incision.

Mouse carotid artery ligation

Mice were anesthetized and LCAs were exposed as described above. The LCAs were completely ligated at the proximal end of the carotid bifurcation with a 6-0 silk suture. The arteries were harvested at 14 or 21 d after surgery. The RCAs were used as sham operation group. The morphological changes were confirmed by HE staining and immunofluorescence staining.

Blood pressure measurement

Blood pressure of mice was monitored with a noninvasive tail-cuff system (Softron BP-98A; Softron, Tokyo, Japan). Mice were trained for 1 week to be acquainted with the measurement. Blood pressure values were averaged from at least three consecutive measurements for each mouse.

Immunofluorescence and morphological staining

Sections embedded in OCT and cells grown on the chamber (Cat NO. 154534, ThermoFisher Scientific, Grand Island, NY, USA) were fixed with paraformaldehyde after washed with PBS for three times. Immunofluorescent staining for α-SMA (Cell Signaling Technology, Cat NO. 19245, Rabbit), α-SMA (Sigma, Cat NO. A2547, Mouse), PCNA (Proteintech, Cat NO. 10205-2-AP), PTPN14 (Santa Cruz Biotechnology, Cat NO. sc-373766), and p-PDGFRβ^{Y692} (GeneScript, Cat. NO. SC2039-PF) was performed as described[33]. The nuclei was stained with DAPI (ZLI-9557, ZSGB-BIO, Beijing, China). Confocal immunofluorescence images were captured by Zeiss confocal laser scanning microscopy. For morphological staining, sections from tissues were stained with hematoxylin and eosin (HE) and the images were analyzed with Image Pro Plus (Media Cybernetics, Rockville, MD, USA).

Cell culture

The human aortic smooth muscle cell line T/G HA-VSMCs (Cat NO. CRL-1999) was from ATCC (Manassas, VA, USA). HA-VSMCs were cultured in Dulbecco's modified Eagle's medium (DMEM)/F12 supplemented with 10% fetal bovine serum in a humidified incubator at 37 °C with 5% CO_2. Cells at passages 4–7 were used in experiments. Before the stimulation with PDGF-BB, the VSMCs underwent starvation with serum-free DMEM for 48 h. HEK293T (Cat NO. CRL-11268, ATCC) cells were cultured in DMEM medium with 10% fetal bovine serum.

Recombinant adenovirus construction and transfection

The adenovirus expressing Flag-tagged human PTPN14 (NM_005401, AdPTPN14), Flag-tagged PTPN14^{C1121S}, Flag-tagged human PDGFRβ (NM_002609, AdPDGFRβ), Flag-tagged PDGFRβ mutants (AdPDGFRβ^{Y692F}, AdPDGFRβ^{Y692D}), and control empty vector (AdNC) were constructed in GeneChem (Shanghai, China). HA-VSMCs were infected with adenovirus at multiplicity of infection (MOI) 10 for 48 h.

Small interfering RNAs (siRNAs) and plasmids transfection

SiRNA targeting PTPN14 (Cat NO. sc-62777) and siRNA control (Cat NO. sc-37007) was from Santa Cruz Biotechnology (Santa Cruz, CA, USA). The siRNA targeting PTPN14 used in Supplementary Figs. 7A, B, 8G, H, and 10A, B were obtained from Sangon Biotech (Shanghai, China). The sequences of siRNA were listed in Supplementary Table 2. HA-VSMCs were pre-incubated in the transfection medium (Opti-MEM, Cat NO. 31985070, Thermo Fisher Scientific) and then transiently transfected with siRNAs by Lipofectamine™ RNAiMAX (Cat NO. 13778150, Thermo Fisher Scientific).

The plasmids of full-length PTPN14, full-length PDGFRβ, and PDGFRβ mutants were constructed by GENEWIZ (Suzhou, China). The PDGFRβ domain truncations were constructed by GeneChem (Shanghai, China). These plasmids were transfected into HEKT293T cells by using Lipofectamine3000 (Cat NO. L3000-015, Thermo Fisher Scientific) for 48 h.

Western blots analysis

HA-VSMCs and aortic tissues were lysed in ice-cold RIPA buffer (Cat NO. P0013B, Beyotime Biotechnology, Beijing, China) containing 1% PMSF (Cat NO. P0100, Solarbio Life Sciences, Beijing, China), 1×protease inhibitor cocktail (Cat NO. 04693132001, Roche, Indianapolis, IN, USA) and phosphatase inhibitor (Cat NO. 04906845001, Roche). After sonication and centrifugation, the concentration of supernatants was measured with BCA protein assay (Cat NO. 23227, Thermo Fisher Scientific). Protein extracts were subjected to SDS–PAGE, transferred to polyvinylidene difluoride membranes (Roche). Analysis involved the primary antibodies for PDGFRβ (Cat NO. 3169, Cell Signaling Technology), α-SMA (Cat NO. 19245, Cell Signaling Technology), SM22 (Cat NO. 40471, Cell Signaling Technology), Flag (Cat NO. 14793, Cell Signaling Technology), Myc (Cat NO. 2276, Cell Signaling Technology), HA (Cat NO. 3724, Cell Signaling Technology), PDGFRα (Cat NO. 3174, Cell Signaling Technology), actin (Cat NO. 3700, Cell Signaling Technology), p-PDGFRβ^{Y692} (Cat. NO. SC2039-PF, GeneScript), AKT (Cat NO. 4691, Cell Signaling Technology), p-AKT (Cat NO. 4060, Cell Signaling Technology), α-Tubulin (Cat NO. 3873, Cell Signaling Technology), PTPN14 (Cat NO. sc-373766, Santa Cruz Biotechnology), ERK1/2

https://doi.org/10.1038/s41467-024-51881-x

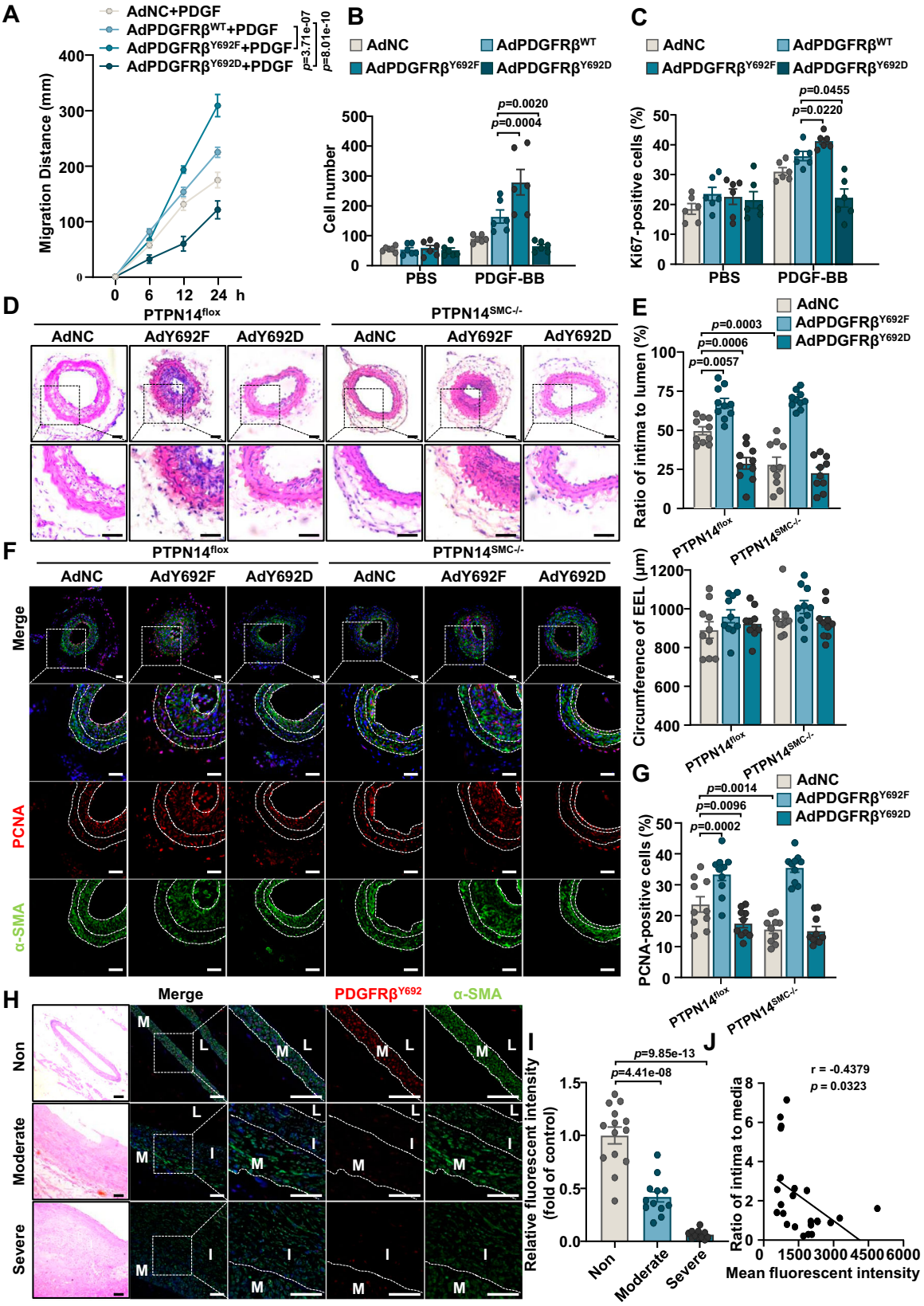

(Cat NO. sc-135900, Santa Cruz Biotechnology), p-ERK1/2 (Cat NO. Sc-7383, Santa Cruz Biotechnology), CNN1 (Cat NO. 24855-1-AP, Proteintech), PCNA (Cat NO. 10205-2-AP, Proteintech), OPN (Cat NO. 22952-1-AP, Proteintech), VIM (Cat NO. 10366-1-AP, Proteintech) and GAPDH (Cat NO. 60004-1-Ig, Proteintech). The dilution ratio used for all primary antibodies was 1.1000. Proteins were visualized with HRP-conjugated anti-rabbit or anti-mouse IgG (1:2000 or 1:8000; Cell Signaling Technology), followed by use of the ECL chemiluminescence system (Cell Signaling Technology). The images were analyzed by using Image J v1.52.

Fig. 8 | Y692 phosphorylation of PDGFRβ alleviated wire injury-induced neointimal hyperplasia. A–**C** Human aortic smooth muscle cells (HA-VSMCs) were transfected with AdPDGFRβ, AdPDGFRβ^{Y692F}, and AdPDGFRβ^{Y692D} for 48 h, following PDGF-BB (20 ng/mL) stimulation for the indicated time. Cell migration was evaluated with scratch assay (**A**) and Transwell assay (**B**), and cell proliferation was assessed with Ki67 staining (**C**). Quantification analysis was presented respectively. The data were presented as the means ± SEM, $n = 6$ (two-way ANOVA with Bonferroni multiple comparison post-hoc test). **D**–**G** PTPN14$^{SMC-/-}$ and PTPN14^{flox} mice subjected to wire injury in left carotid arteries (LCAs) were transfected with AdNC, AdPDGFRβ^{Y692F}, or AdPDGFRβ^{Y692D} for 14 d. **D**, **E** Representative HE staining of cross-sections of LCAs of mice. Scale bar, 50 μm. Quantification analysis of the ratios of intima to lumen, and the circumference of external elastic lamina (EEL) in the cross-sections from the LCAs at 14 d post-injury. The data were presented as the means ± SEM, $n = 10$ (one-way ANOVA with Bonferroni multiple comparison post-hoc test). **F**, **G** Representative immunofluorescence staining and quantification of the percentage of PCNA-positive cells in cross-sections of LCAs. PCNA, red; α-SMA, green; DAPI, blue. Scale bar, 50 μm. The data were presented as the means ± SEM, $n = 10$ (one-way ANOVA with Bonferroni multiple comparison post-hoc test). **H** Representative HE and immunofluorescence staining of phosphor-PDGFRβ^{Y692} in the human coronary arteries. PDGFRβ^{Y692}, red; α-SMA, green; DAPI, blue. Scale bar, 50 μm. **I** Quantification of the expression levels of phosphor-PDGFRβ^{Y692}. The data were presented as the means ± SEM. $n = 14, 13, 11$, respectively. (one-way ANOVA with Bonferroni multiple comparison post-hoc test). **J** The Correlation Analysis between the levels of phosphor-PDGFRβ^{Y692} and the degree of intimal hyperplasia in human coronary arteries, $n = 24$ (two-tailed nonparametric Spearman correlation). L: Lumen, M: Media, I: Intima.

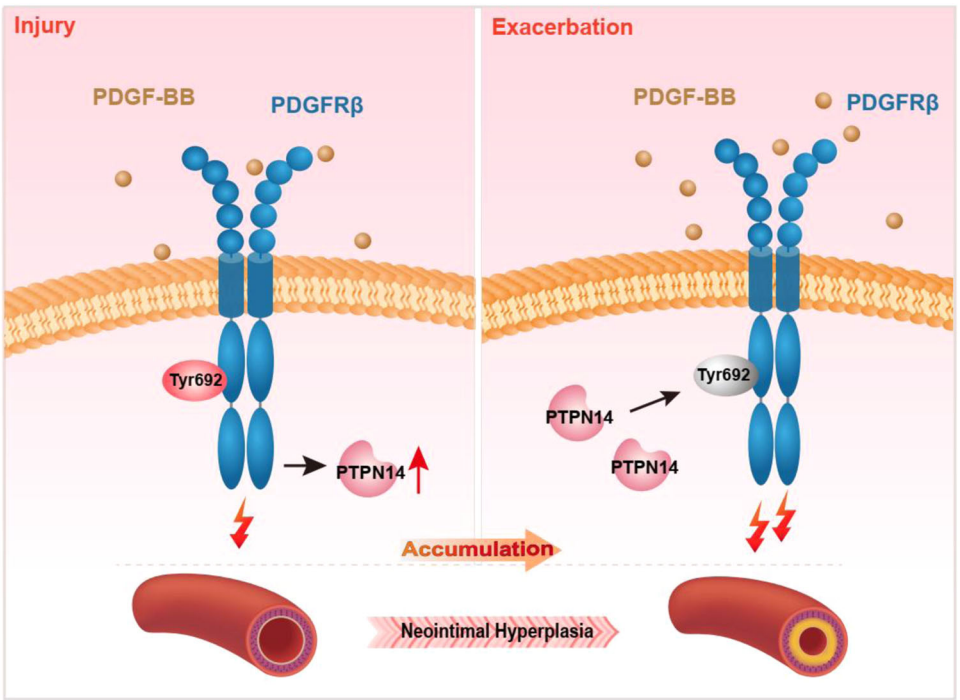

Fig. 9 | Schematic illustration of the PTPN14/PDGFRβ^{Y692} cascade in VSMC phenotypic modulation and neointima formation. After vessel injury, PDGF-BB induces the expression of PTPN14, which dephosphorylates the inhibitory phosphorylation site of PDGFRβ at Y692, in VSMCs. Subsequently, dephosphorylation of PDGFRβ^{Y692} leads to augmentation of PDGF-BB-induced PDGFRβ signaling activation, which finally promotes VSMC phenotypic modulation and aggravates neointimal hyperplasia.

Total RNA extraction and quantitative real-time PCR (qRT-PCR) analysis

Total RNA of cells and tissues was extracted by using kit (Cat NO. 15596018, Thermo Fisher Scientific) according to the manufacturer's instructions. RNA samples were reverse-transcribed with SuperScript III and random primers (Cat NO. 12574035, Thermo Fisher Scientific). qRT-PCR was performed with SYBR Green PCR master mix (Cat NO. AQ131-01, TransGen Biotech, Beijing) and the ABI 7900HT Real-Time PCR System (Life Technologies, CA, USA). Primers sequences were listed in Supplementary Table 3.

Immunoprecipitation assay

Cells were collected with ice-cold IP lysis (50 mM Tris-HCl, 150 mM NaCl, 1% Nonidet-P40) containing 1% PMSF, 1×protease inhibitor cocktail (Cat NO. 04693132001, Roche), and phosphatase inhibitor (Cat NO. 04906845001, Roche). For endogenous immunoprecipitation with HA-VSMCs, the cell lysates were incubated with primary antibodies at 4 °C overnight. The lysates incubated with IgG antibody were served as negative controls. After washing and centrifugation with IP buffer for three times, Protein A/G PLUS-Agarose beads (Cat NO. 20423, Thermo Fisher Scientific) was added in the lysates for reaction at room temperature for 2 h. After a final wash, the supernatant was discarded, and the precipitated proteins were eluted from the beads by resuspending in 1× SDS-PAGE loading buffer. For immunoprecipitation with HEK293T cells, the cells lysates were immunoprecipitated with anti-Flag (Cat NO. B26101, Bimake, Shanghai) or anti-Myc (Cat NO. B26301, Bimake) affinity beads at 4 °C overnight. The dilution ratio used for all antibodies was 1:100. The resultant materials from immunoprecipitation or cell lysates underwent western blot analysis.

Phosphatase assay

The phosphatase activity of PTPN14 was assessed with RediPlate 96 EnzChek Tyrosine Phosphatase Assay kit (Cat NO. R22067, Thermo

Fisher Scientific)[56]. Briefly, PTPN14 was immunoprecipitated from tissue or HA-VSMCs lysates by incubating with PTPN14 antibody, which was bounding to Protein A/G PLUS-Agarose beads. The protein complex was collected with tyrosine phosphatase reaction buffer after washing beads three times with IP buffer. The complex and tyrosine phosphatase reaction buffer were added into RediPlate wells and incubated for 30 min at 37 °C. A fluorescence microplate reader equipped with appropriate filters (excitation = 355 nm, emission = 460 nm) was employed to detect the fluorescence.

RNA-sequencing analysis

The total RNA was collected from HA-VSMCs followed by knockout of PTPN14 and PDGF-BB treatment. TRIzol reagent was used to isolate RNA. The RNA sequencing database was conducted by BGI (Shenzhen, China). Heatmap of differentially expressed genes was generated by MetaboAnalyst (http://www.metaboanalyst.ca). Cytoscape software (version 3.8.0) was used to construct a visual network to show the functions enriched by differential genes.

Mass spectrometry analysis

Mass spectrometry was used to identify the potential phosphorylation sites in PDGFRβ. Briefly, HA-VSMCs were transfected with PTPN14 siRNA and AdPDGFRβ for 48 h. After the stimulation with PDGF-BB (10 ng/mL) for 10 min, the cells were isolated with IP lysis and purified with tagged-Myc affinity beads. With the SDS-PAGE western blot assay and Coomassie Blue staining, the specific bands enriched intensive signals were cut out. The gels were subjected to in-gel tryptic digestion and further analyzed by reverse-phase nano-LC-MS/MS (Q-Exactive mass spectrometer, Thermo Fisher Scientific). Proteome Discoverer engine (v 1.3, Thermo Fisher Scientific) was used to analyze the results and to identify the phosphorylation sites.

Proximity ligation assay (PLA)

Sections from tissues were embedded with OCT and washed with wash buffer for three times. After fixed with paraformaldehyde, the sections were permeabilized with 0.1 % Triton X-100 for 30 min, then blocked with goat serum for 30 min following by washing with wash buffer. Incubation with primary antibodies against SM22 (Cat NO. ab150129, Abcam), PDGFRβ (Cat NO. MB64422, Bioworld), or PDGF-B (Cat NO. AF0240, Affinity) at 4 °C overnight. The dilution ratio used for all antibodies was 1:200. Subsequently, the staining was performed by using the Rabbit PLUS and Mouse MINUS Duolink in situ PLA kits (Cat NO. DUO92101, Sigma-Aldrich) according to the manufacturer's protocol. The nuclei were counterstained with DAPI. Immunofluorescent signals were captured by Zeiss confocal laser scanning microscopy.

Proliferation assay

The proliferation ability of the HA-VSMCs was demonstrated by Ki67 staining. After knockdown or overexpression performance, HA-VSMCs were seeded into chamber until they grew to approximately 70% confluence, then underwent serum-free overnight starvation and stimulated with PDGF-BB (20 ng/mL) for 24 h. With fixation, permeabilization, and blocking, the cells were incubated with Ki67 antibody (Cat NO. 11882, Cell Signaling Technology) at 4 °C overnight. After washing with PBS, F-actin filaments were labeled with DyLight™ 594 Phalloidin (Cat NO. 12877, Cell Signaling Technology) for 30 min. The dilution ratio used for antibodies was 1:200. The nuclei were stained with DAPI. The immunofluorescent images were scanning with Zeiss confocal laser scanning microscopy.

Migration assay

Scratch wound healing assays and Transwell assays were performed to evaluate migration ability of HA-VSMCs. For Scratch wound healing assays, HA-VSMCs were grown in 6-well plates with DMEM/F12 supplemented with 10% fetal bovine serum. HA-VSMCs were pretreated with serum-free DMEM for 48 h. A blank area with a 200 μL pipette tip was artificially framed on the cell plate and the floating cell debris was removed. Then the cells were cultured in serum-free DMEM with or without PDGF-BB (20 ng/mL). The images were captured at 0, 6, 12, 24 h in a fixed position.

In Transwell assays, HA-VSMCs were seeded in 8.0 μm Transwells (Cat NO. 353097, BD Falcon) with treatment of PDGF-BB (20 ng/mL). After 6 h migration, the upper insert was washed with PBS and fixed with paraformaldehyde. The cells were counterstained with DAPI following by removing the cells on the upper surface. The images were randomly selected with fluorescence microscope and analyzed with Image Pro Plus software.

Protein purification and surface plasmon resonance assay

Recombinant PDGFRβ (1-702aa) and PDGFRβ^{Y692D} (1-702aa with a mutation of Y692D) proteins were from GenScript (Piscataway, NJ, United States). Briefly, target DNA sequence of human PDGFRβ was synthesized and then subcloned into target vector for insect cell expression. DH10Bac strain was used for the recombinant bacmid (rbacmid) generation. The positive rbacmid containing PDGFRβ sequence gene was confirmed by PCR. The Sf9 cells were infected with P2 virus at 3 MOIs (0.5, 3, 10) at 22/27 °C and harvested at three time point (48 h, 72 h, 96 h) to obtain the maximum expression level. Western blot was used to monitor the expression. After solubilization screening of detergent, 1 L Sf9 cell culture were infected by P2 virus at MOI 10. Cells were incubated in Sf-900II SFM (1×) for 48 h at 22 °C before harvest. Cell pellets were harvested, washed, and lysed with 20 mM Chaps, rotated for 3 h at 4 °C at a gentle rpm, and then centrifuged at 15,000 rpm for 10 min at 4 °C. The supernatant was incubated with Ni-NTA Resin to capture the target protein. Higher purity fractions were pooled and dialyzed in 50 mM Tris-HCl, 500 mM NaCl, 5% Glycerol, 2 mM CHAPS, pH 8.0, then followed by 0.22 μm filter sterilization.

The binding affinity of PDGF/PDGFRβ was performed using BIAcore T200 system (GE Healthcare, Uppsala, Sweden). Briefly, recombinant PDGFRβ protein was covalently immobilized on CM5 sensor chip with the amine coupling kit provided by the manufacture until achieved approximately 1000 RUs. Analytes (PDGF-BB/PDGF-DD) were run using HBS buffer solution and flowed through the chip. The measuring parameters including association (ka), dissociation (kd) rate constants and binding affinities (K_D) were calculated using the Biacore evaluation software (T200 version 3.0).

Cross-linking of PDGFRβ dimers

For analyzing the PDGFRβ dimerization, cells were starved in serum-free medium overnight, followed by stimulation with PDGF-BB (50 ng/mL) for 30 min. Cross-link reaction was performed by the addition of 100 μM disuccinimidyl suberate (DSS) and the incubation at room temperature for 30 min. The cell lysates were collected with lysis and analyzed by SDS-PAGE and western blot.

Human samples

Studies using human coronary arteries samples[57,58] were approved by the Ethics Committee of Tianjin Medical University and family members of subjects provided written informed consent for autopsy. The arterial samples were divided into non-hyperplastic and hyperplastic arteries based on their morphology. HE and immunofluorescence staining were performed as described above.

Statistical analysis

The statistical data was presented as means ± SEM. The data were tested for normality before parametric statistics using the Shapiro-Wilk normality test ($n \geq 6$). For normally distributed data, we

conducted comparisons between two groups using the unpaired Student's *t* test, whereas three or more groups were analyzed using the one-way ANOVA followed by the Bonferroni's multiple comparisons test. For non-normal data or a small sample size ($n < 6$), we utilized the Mann–Whitney *U* test or the Kruskal-Wallis test followed by the Dunn's multiple comparison test. Furthermore, for data with two or more subcategories, we employed a two-way ANOVA followed by the Bonferroni's multiple comparison test. The correlations between PTPN14/restenosis and PDGFRβ^{Y692}/restenosis in human atherosclerotic plaques was determined by Spearman's rank test. All the statistical analysis was performed with Graphpad Prism 9.0 software. *P* value < 0.05 was considered statistically significant. The sample size for each experiment was indicated in the figure legend.

Reporting summary

Further information on research design is available in the Nature Portfolio Reporting Summary linked to this article.

Data availability

Data supporting the findings of this study are available in the article, its Supplementary information, the source data file and from the corresponding author upon request. The RNA-sequencing data has been submitted to GEO datasets (GSE267140). Source data are provided with this paper.

References

1. Basatemur, G. L., Jorgensen, H. F., Clarke, M. C. H., Bennett, M. R. & Mallat, Z. Vascular smooth muscle cells in atherosclerosis. *Nat. Rev. Cardiol.* **16**, 727–744 (2019).
2. Owens, G. K., Kumar, M. S. & Wamhoff, B. R. Molecular regulation of vascular smooth muscle cell differentiation in development and disease. *Physiol. Rev.* **84**, 767–801 (2004).
3. Millette, E. et al. Platelet-derived growth factor-BB-induced human smooth muscle cell proliferation depends on basic FGF release and FGFR-1 activation. *Circ. Res.* **96**, 172–179 (2005).
4. Chen, P. Y. et al. Smooth Muscle Cell Reprogramming in Aortic Aneurysms. *Cell Stem Cell* **26**, 542–557.e11 (2020).
5. Jawien, A., Bowen-Pope, D. F., Lindner, V., Schwartz, S. M. & Clowes, A. W. Platelet-derived growth factor promotes smooth muscle migration and intimal thickening in a rat model of balloon angioplasty. *J. Clin. Invest.* **89**, 507–511 (1992).
6. Tonks, N. K. Protein tyrosine phosphatases: from genes, to function, to disease. *Nat. Rev. Mol. Cell Bio* **7**, 833–846 (2006).
7. Smith, A. L. et al. Pez: a novel human cDNA encoding protein tyrosine phosphatase- and ezrin-like domains. *Biochem. Biophys. Res. Commun.* **209**, 959–965 (1995).
8. Barr, A. J., Debreczeni, J. E., Eswaran, J. & Knapp, S. Crystal structure of human protein tyrosine phosphatase 14 (PTPN14) at 1.65-A resolution. *Proteins* **63**, 1132–1136 (2006).
9. Belle, L. et al. The tyrosine phosphatase PTPN14 (Pez) inhibits metastasis by altering protein trafficking. *Sci. Signal* **8**, ra18 (2015).
10. Ogata, M. et al. Regulation of phosphorylation level and distribution of PTP36, a putative protein tyrosine phosphatase, by cell-substrate adhesion. *J. Biol. Chem.* **274**, 20717–20724 (1999).
11. Ogata, M. et al. Effects of overexpression of PTP36, a putative protein tyrosine phosphatase, on cell adhesion, cell growth, and cytoskeletons in HeLa cells. *J. Biol. Chem.* **274**, 12905–12909 (1999).
12. Yang, Y. et al. Harmine alleviates atherogenesis by inhibiting disturbed flow-mediated endothelial activation via protein tyrosine phosphatase PTPN14 and YAP. *Br. J. Pharm.* **178**, 1524–1540 (2021).
13. Mao, C. et al. Nidogen-2 Maintains the Contractile Phenotype of Vascular Smooth Muscle Cells and Prevents Neointima Formation via Bridging Jagged1-Notch3 Signaling. *Circulation* **144**, 1244–1261 (2021).
14. Fu, P. et al. Phospholipase D2 restores endothelial barrier function by promoting PTPN14-mediated VE-cadherin dephosphorylation. *J. Biol. Chem.* **295**, 7669–7685 (2020).
15. Díaz-Valdivia, N. I. et al. The non-receptor tyrosine phosphatase type 14 blocks caveolin-1-enhanced cancer cell metastasis. *Oncogene* **39**, 3693–3709 (2020).
16. Yun, H. Y. et al. Structural basis for recognition of the tumor suppressor protein PTPN14 by the oncoprotein E7 of human papillomavirus. *PLoS Biol.* **17**, e3000367 (2019).
17. Alexander, M. R. & Owens, G. K. Epigenetic control of smooth muscle cell differentiation and phenotypic switching in vascular development and disease. *Annu Rev. Physiol.* **74**, 13–40 (2012).
18. Au, A. C. et al. Protein tyrosine phosphatase PTPN14 is a regulator of lymphatic function and choanal development in humans. *Am. J. Hum. Genet* **87**, 436–444 (2010).
19. Wyatt, L., Wadham, C., Crocker, L. A., Lardelli, M. & Khew-Goodall, Y. The protein tyrosine phosphatase Pez regulates TGFbeta, epithelial-mesenchymal transition, and organ development. *J. Cell Biol.* **178**, 1223–1235 (2007).
20. Paul, M. D. & Hristova, K. The RTK Interactome: Overview and Perspective on RTK Heterointeractions. *Chem. Rev.* **119**, 5881–5921 (2019).
21. Andrae, J., Gallini, R. & Betsholtz, C. Role of platelet-derived growth factors in physiology and medicine. *Genes Dev.* **22**, 1276–1312 (2008).
22. Verstraete, K. & Savvides, S. N. Extracellular assembly and activation principles of oncogenic class III receptor tyrosine kinases. *Nat. Rev. Cancer* **12**, 753–766 (2012).
23. Lemmon, M. A. & Schlessinger, J. Cell signaling by receptor tyrosine kinases. *Cell* **141**, 1117–1134 (2010).
24. Alonso, A. et al. Protein tyrosine phosphatases in the human genome. *Cell* **117**, 699–711 (2004).
25. Yu, Z. H. & Zhang, Z. Y. Regulatory Mechanisms and Novel Therapeutic Targeting Strategies for Protein Tyrosine Phosphatases. *Chem. Rev.* **118**, 1069–1091 (2018).
26. Tonks, N. K. Protein tyrosine phosphatases: from genes, to function, to disease. *Nat. Rev. Mol. Cell Biol.* **7**, 833–846 (2006).
27. Sevillano, J., Sanchez-Alonso, M. G., Pizarro-Delgado, J. & Ramos-Alvarez, M. D. P. Role of Receptor Protein Tyrosine Phosphatases (RPTPs) in Insulin Signaling and Secretion. *Int J. Mol. Sci.* **22**, 5812 (2021).
28. Chang, Y., Zhuang, D., Zhang, C. & Hassid, A. Increase of PTP levels in vascular injury and in cultured aortic smooth muscle cells treated with specific growth factors. *Am. J. Physiol. Heart Circ. Physiol.* **287**, H2201–H2208 (2004).
29. Chang, Y. et al. Counter-regulatory function of protein tyrosine phosphatase 1B in platelet-derived growth factor- or fibroblast growth factor-induced motility and proliferation of cultured smooth muscle cells and in neointima formation. *Arterioscler Thromb. Vasc. Biol.* **26**, 501–507 (2006).
30. Qi, W. et al. SHP-1 activation inhibits vascular smooth muscle cell proliferation and intimal hyperplasia in a rodent model of insulin resistance and diabetes. *Diabetologia* **60**, 585–596 (2017).
31. Gong, H. et al. Shp2 in myocytes is essential for cardiovascular and neointima development. *J. Mol. Cell Cardiol.* **137**, 71–81 (2019).
32. Chen, K. E. et al. Substrate specificity and plasticity of FERM-containing protein tyrosine phosphatases. *Structure* **23**, 653–664 (2015).
33. He, J. et al. Yes-Associated Protein Promotes Angiogenesis via Signal Transducer and Activator of Transcription 3 in Endothelial Cells. *Circ. Res.* **122**, 591–605 (2018).

34. Franklin, J. M., Wu, Z. & Guan, K. L. Insights into recent findings and clinical application of YAP and TAZ in cancer. *Nat. Rev. Cancer* **23**, 512–525 (2023).
35. Huang, J. M. et al. YAP modifies cancer cell sensitivity to EGFR and survivin inhibitors and is negatively regulated by the non-receptor type protein tyrosine phosphatase 14. *Oncogene* **32**, 2220–2229 (2013).
36. Mello, S. S. et al. A p53 Super-tumor Suppressor Reveals a Tumor Suppressive p53-Ptpn14-Yap Axis in Pancreatic Cancer. *Cancer Cell* **32**, 460–473.e6 (2017).
37. Liu, X. et al. PTPN14 interacts with and negatively regulates the oncogenic function of YAP. *Oncogene* **32**, 1266–1273 (2013).
38. Knight, J. F. et al. KIBRA (WWC1) Is a Metastasis Suppressor Gene Affected by Chromosome 5q Loss in Triple-Negative Breast Cancer. *Cell Rep.* **22**, 3191–3205 (2018).
39. Wang, W. et al. PTPN14 is required for the density-dependent control of YAP1. *Genes Dev.* **26**, 1959–1971 (2012).
40. Xie, C. et al. Yap1 protein regulates vascular smooth muscle cell phenotypic switch by interaction with myocardin. *J. Biol. Chem.* **287**, 14598–14605 (2012).
41. Wang, X. et al. The induction of yes-associated protein expression after arterial injury is crucial for smooth muscle phenotypic modulation and neointima formation. *Arterioscler Thromb. Vasc. Biol.* **32**, 2662–2669 (2012).
42. Osman, I. et al. YAP1/TEAD1 upregulate platelet-derived growth factor receptor beta to promote vascular smooth muscle cell proliferation and neointima formation. *J. Mol. Cell. Cardiol.* **156**, 20–32 (2021).
43. Wadham, C., Gamble, J. R., Vadas, M. A. & Khew-Goodall Y The protein tyrosine phosphatase Pez is a major phosphatase of adherens junctions and dephosphorylates beta-catenin. *Mol. Biol. Cell* **14**, 2520–2529 (2003).
44. Zhang, P. et al. Identification and functional characterization of p130Cas as a substrate of protein tyrosine phosphatase non-receptor 14. *Oncogene* **32**, 2087–2095 (2013).
45. Choi, J., Saraf, A., Florens, L., Washburn, M. P. & Busino, L. PTPN14 regulates Roquin2 stability by tyrosine dephosphorylation. *Cell Cycle* **17**, 2243–2255 (2018).
46. Lonic, A. et al. Phosphorylation of PKCδ by FER tips the balance from EGFR degradation to recycling. *J. Cell Biol.* **220**, e201902073 (2021).
47. Matsui, T. et al. Isolation of a novel receptor cDNA establishes the existence of two PDGF receptor genes. *Science* **243**, 800–804 (1989).
48. Wu, J. H. et al. The platelet-derived growth factor receptor-beta phosphorylates and activates G protein-coupled receptor kinase-2. A mechanism for feedback inhibition. *J. Biol. Chem.* **280**, 31027–31035 (2005).
49. He, C. et al. PDGFRβ signalling regulates local inflammation and synergizes with hypercholesterolaemia to promote atherosclerosis. *Nat. Commun.* **6**, 7770 (2015).
50. Farrar, C. S. & Hocking, D. C. Assembly of fibronectin fibrils selectively attenuates platelet-derived growth factor-induced intracellular calcium release in fibroblasts. *J. Biol. Chem.* **293**, 18655–18666 (2018).
51. Pham, T., Najy, A. J. & Kim, H. C. E3 ligase HUWE1 promotes PDGF D-mediated osteoblastic differentiation of mesenchymal stem cells by effecting polyubiquitination of β-PDGFR. *J. Biol. Chem.* **298**, 101981 (2022).
52. Rorsman, C., Tsioumpekou, M., Heldin, C. H. & Lennartsson, J. The Ubiquitin Ligases c-Cbl and Cbl-b Negatively Regulate Platelet-derived Growth Factor (PDGF) BB-induced Chemotaxis by Affecting PDGF Receptor β (PDGFRβ) Internalization and Signaling. *J. Biol. Chem.* **291**, 11608–11618 (2016).
53. Kramer, F. et al. Platelet-derived growth factor receptor β activation and regulation in murine myelofibrosis. *Haematologica* **105**, 2083–2094 (2020).
54. Chiara, F., Bishayee, S., Heldin, C. H. & Demoulin, J. B. Auto-inhibition of the platelet-derived growth factor beta-receptor tyrosine kinase by its C-terminal tail. *J. Biol. Chem.* **279**, 19732–19738 (2004).
55. Irusta, P. M. & DiMaio, D. A single amino acid substitution in a WW-like domain of diverse members of the PDGF receptor subfamily of tyrosine kinases causes constitutive receptor activation. *EMBO J.* **17**, 6912–6923 (1998).
56. Dubois, M. J. et al. The SHP-1 protein tyrosine phosphatase negatively modulates glucose homeostasis. *Nat. Med.* **12**, 549–556 (2006).
57. Li, B. et al. c-Abl regulates YAPY357 phosphorylation to activate endothelial atherogenic responses to disturbed flow. *J. Clin. Invest.* **129**, 1167–1179 (2019).
58. Wang, Q. et al. Soluble epoxide hydrolase is involved in the development of atherosclerosis and arterial neointima formation by regulating smooth muscle cell migration. *Am. J. Physiol. Heart Circ. Physiol.* **309**, H1894–H1903 (2015).

Acknowledgements

This work was supported by National Key Research and Development Program of China Grant (2019YFA0802003 to Y.Z. and 2022YFE0131400 to M.L.) and National Natural Science Foundation of China Grants (82330012 and 82127808 to Y.Z.; 82220108014 to M.L.; 82270516 and 82070451 to J.H.). The authors thank Dr. Wen Wei (Biodesign Center for Mechanisms of Evolution, Arizona State University) for his assistance in conducting the Gene Set Enrichment Analysis.

Author contributions

Q.M. and X.H. performed the experiments and statistical analysis. X.W. and G.Z. helped with animal study. Y.Z. performed plasmid construction. C.S. and M.W. performed human specimen analysis. K.Z. provided technical help in mass spectrometry analysis. J.H., Y.Z., and M.L. conceived the studies and supervised the project. J.H., Y.Z., and Q.M. contributed to the interpretation of data and manuscript. All the authors contributed to the final version.

Competing interests

The authors declare no competing interests.

Additional information

Supplementary information The online version contains supplementary material available at https://doi.org/10.1038/s41467-024-51881-x.

Correspondence and requests for materials should be addressed to Ming Liu, Yi Zhu or Jinlong He.

Peer review information *Nature Communications* thanks Jin-Kun Wen, and the other, anonymous, reviewer(s) for their contribution to the peer review of this work. A peer review file is available.